EVALUATIONS OF FIRE-RETARDANT FIBER-REINFORCED POLYMER MATERIALS FOR BUILDING APPLICATIONS

A Thesis

Presented in Partial Fulfillment of the Requirements for the

Degree of Master of Science

with a

Major in Civil Engineering

in the

College of Graduate Studies

University of Idaho

by

Michaela R. Petersen

May 2014

Major Professor: An Chen, Ph.D.

Authorization to Submit Thesis

This thesis of Michaela R. Petersen, submitted for the degree of Master of Science with a Major in Civil Engineering and titled, "Evaluations of Fire-Retardant Fiber-Reinforced Polymer Materials for Building Applications," has been reviewed in final form. Permission, as indicated by the signatures and dates below, is now granted to submit final copies to the College of Graduate Studies for approval.

Major Professor: _____ Date: _____
An Chen, Ph.D.

Committee
Members: _____ Date: _____
Mark Roll, Ph.D.

_____ Date: _____
Richard Nielsen, Ph.D.

_____ Date: _____
Pizhong Qiao, Ph.D.

Department
Administrator: _____ Date: _____
Richard Nielsen, Ph.D.

Discipline's
College Dean: _____ Date: _____
Larry Stauffer, Ph.D.

Final Approval and Acceptance

Dean of the College
of Graduate Studies: _____ Date: _____
Jie Chen, Ph.D.

Abstract

Fiber reinforced polymer (FRP) is a lightweight building material which provides a low weight-to-strength ratio. Applications in civil engineering include providing a lightweight alternative to steel reinforcement in concrete, as well as to stiffen wood, etc. However, there has been no study to determine methods to alter FRP so that it satisfies the International Building Code's (IBC) standards for fire-resistance. Therefore, this thesis' goal is to determine a method of altering the resin in FRP to achieve the fire resistance standards of the IBC. In order to do this, different additives were tested for flame-spread, time to ignition and time to self-extinguish, and then the optimal additive was selected and tested for its effects on the mechanical properties of the composite. From this, it was found that adding 25% Alumina-Tri-Hydrate by weight satisfies the fire-resistive standards while only slightly reducing the mechanical properties of the composite.

Acknowledgements

I would like to thank the following people for their support and help and advice during the time that I was running tests and writing my thesis.

First I would like to thank my major professor, Dr. Chen, and my committee members, Dr. Roll, Dr. Qiao and Dr. Nielsen, for providing guidance, support, and troubleshooting advice.

Next I would like to thank Don Parks for assisting me in shop related needs. Thanks go to Dr. Jung for allowing me to use his MTS machine as well as to Dr. Smith, Dr. Qiao and Dr. Odom for allowing me to use their testing fixtures and for providing advice and materials.

I would like to thank all the other graduate students and undergraduate students who helped me in my research. Without your help holding propane torches or cameras I would not have been able to run many of my tests. Specifically, I would like to thank Tony Parris, Nic Pena and Dallas Roberts for always being willing to help me with various experiments no matter how inconveniently scheduled they were. Also, I would like to thank Tom Norris for editing my thesis and Paul Ziegler for teaching me how to use Comsol.

I would like to thank my family. My parents both helped provide tips on formatting as well as how to write a thesis. In addition, they helped keep me motivated and were always willing to babysit my puppy while I was working late.

Last, I would like to thank the Department of Energy for providing financial support for my research.

Table of Contents

Authorization to Submit Thesis ii
Abstract iii
Acknowledgements iv
Table of Contents v
List of Figures vii
List of Tables ix
Chapter 1: Introduction 1
Chapter 2: A Study of the International Building Code 3
2.1 Introduction 3
2.2 International Building Code Requirements 3
2.2.1 Requirements as a Load Bearing Member 3
2.3 FRP as an Interior Finish 8
2.3.1 FRP as a Roofing Material 10
2.3.2 Requirements for Foam Insulation and FRP 12
2.4 Summary 14
Chapter 3: A Literature Review of FRP and Polystyrene as Building Materials 15
3.1 Introduction 15
3.2 Structural 15
3.3 Materials 17
3.4 Conclusion 20
Chapter 4: Thermodynamic Properties of the FRP and Polystyrene 21
4.1 Introduction 21
4.2 Testing (Preliminary ASTM E 108) 22
4.2.1 Specimen Setup 22
4.3 Results 24
4.3.1 Fire Results 24
4.3.2 Smoke Results 29
4.3.3 Char formation 32
4.3.4 Workability Limit 32
4.3.4 Special Resin Flame Test 35

4.4 Panel Tests (Preliminary ASTM E 119) 35
4.4.1 Single Panel Tests 35
4.4.2 Double Panel Tests 42
4.5 Flame Spread Tests (Preliminary ASTM E 84) 44
4.5.1 Introduction 44
4.6 Mathematical Model 46
4.6.1 Steady State Model 46
4.6.2 Unsteady State Model 47
4.7 Conclusion 52
Chapter 5: Mechanical Tests 54
5.1 Introduction 54
5.2 Samples 54
5.3 Testing - Methods 56
5.3.1 Strain Gage Placement 56
5.3.2 Loading Rates 58
5.3.3 Methods 58
5.4 Results 60
5.4.1 Compression Test (ASTM D 695) 60
5.4.2 Flexural (ASTM D 790) 66
5.3.3 Shear (ASTM C 1292) 71
5.4.4 Tension (ASTM D 638) 74
5.5 Conclusion 78
Chapter 6 – Conclusions and Recommendations 80
Works Cited 81
Appendix A – Additional ASTM Standards 85

List of Figures

Figure 1: Fire resistance vs. % Additives 26
Figure 2: Panel Setup 36
Figure 3: Testing system 36
Figure 4: Changes of the gypsum over two hour at (A) 1 hr, (B) 1.5 hrs, (C)1.83 hrs 37
Figure 5: RR control FRP 38
Figure 6: (A): RR + ATH1 FRP (B): RR + ATH2 FRP 38
Figure 7: Foam melting for (A) RR+ATH1, (B) RR+ATH2 39
Figure 8: Foam melting for RR control 39
Figure 9: Foam melting for FRR control 40
Figure 10: Time vs. Temperature curve for RR control 41
Figure 11: Time vs. Temperature curve between ATH1, ATH2 and FRR Control 41
Figure 12: Top of Gypsum after Double Panel Test 43
Figure 13: Average Double Panel Test 44
Figure 14: Flame Spread Test Setup 45
Figure 15: Unsteady State System 48
Figure 16: Fine Mesh 49
Figure 17: Course Mesh 49
Figure 18: Comsol Convergence Study 49
Figure 19: Influence of Applied Heat 50
Figure 20: Heat Flux through System 51
Figure 21: Temperature with Respect to Position 52
Figure 22: Temperature with Respect to Position, Zoomed in 52
Figure 23: Vacuum Bagging Process A) FRP sealing bag B) After sealing bag 54
Figure 24: Compression Dimensions 55
Figure 25: Flexure Dimensions 55
Figure 26: Shear Dimensions 56
Figure 27: Tension Dimensions 56
Figure 28: Placement of Compression Strain Gage, Example of Compression Fixture 57
Figure 29: Placement of Flexure Strain Gage 57

Figure 30: Placement of Tension Strain Gage 58
Figure 31: Example of Flexure Fixture 59
Figure 32: Example of Shear Fixture 59
Figure 33: Example of Shear Fixture, Failed Tension Sample 60
Figure 34: Force-Displacement Curves for Compression 61
Figure 35: Comparison of Stress-Strain Curves of MTS and DAS for Control 62
Figure 36: Comparison of Stress-Strain Curves of MTS and DAS for 25% ATH 62
Figure 37: Comparison of Stress-Strain Curves of MTS and DAS for 50% ATH 63
Figure 38: Stress-Strain Curves for Compression 63
Figure 39: Comparison for Compressive Modulus of Elasticity 64
Figure 40: Max Compressive Stress with Error Bounds 65
Figure 41: Failure Mode 66
Figure 42: Force-Displacement Curves for Flexure 67
Figure 43: Control Stress-Strain Curve from DAS 68
Figure 44: 50% ATH Stress-Strain Curve from DAS 68
Figure 45: Comparison for Flexural Modulus of Elasticity 69
Figure 46: Max Flexural Stress with Error Bounds 70
Figure 47: Failure Mode, Bottom View of (A) Control, (B) 25% ATH, (C) 50% ATH 70
Figure 48: Failure Mode, Side View of (A) Control, (B) 25% ATH, (C) 50% ATH 71
Figure 49: Force-Displacement Curves for Shear 72
Figure 50: Max Shear Stress with Error Bounds 73
Figure 51: Failure Mode for (A) Control, (B) 25% ATH, (C) 50% ATH 73
Figure 52: Force-Displacement Curves for Tension 74
Figure 53: Comparison of Stress-Strain Curves of MTS and DAS for Control ATH 75
Figure 54: Comparison of Stress-Strain Curves of MTS and DAS for 25% ATH 75
Figure 55: Comparison of Stress-Strain Curves of MTS and DAS for 50% ATH 76
Figure 56: Stress-Strain Curves for Tension 76
Figure 57: Comparison for Tensile Modulus of Elasticity 77
Figure 58: Max Tensile Stress with Error Bounds 78
Figure 59: Failure Mode 78

List of Tables

Table 1: Allowable Building Heights and Stories 4
Table 2: Fire-Resistance Rating Requirements for Building Elements 6
Table 3: Material Testing Standards 7
Table 4: Minimum Roof Covering Classification for Types of Construction 8
Table 5: Roofing Materials Classification 8
Table 6: Interior Wall and Ceiling Finish Requirements by Occupancy 9
Table 7: Material Classification 10
Table 8: FM Approvals Flame Spread Requirements for Above the Roof Deck 11
Table 9: Requirements for Calorimeter Test 12
Table 10: Foam Plastic Insulation Flame Spread Index and Smoke Development Index 13
Table 11: Summary of Required Testing Method 14
Table 12: Resin Properties 21
Table 13: Time to set for additives 23
Table 14: Results from flame test 25
Table 15: Results from Smoke Test 29
Table 16: Formation of Char Layer 32
Table 17: Workability Results for Standard Resin 33
Table 18: Workability Results for Special Resin 34
Table 19: Double Panel Test Information 44
Table 20: Flame spread results 46
Table 21: Steady State Heat Flow Values 47
Table 22: Steady State Temperatures 47
Table 23: Unsteady State Thermal Properties 48
Table 24: Loading Rates 58
Table 25: Maximum Force, Stress and Displacement for Compression 64
Table 26: Average Maximum Force, Stress and Displacement for Flexure 69
Table 27: Average Maximum Force, Stress and Displacement for Shear 72
Table 28: Average Maximum Force, Stress and Displacement for Tension 77
Table 29: Requirements for ASTM C 1029 86

Table 30: Material Requirements 86
Table 31: Requirements for ASTM D 1929 86
Table 32: Requirements for ASTM D 5665 87
Table 33: Requirements for ASTM D 5726 87
Table 34: Requirements for ASTM D 7281 88
Table 35: Requirements for ASTM E 84 88
Table 36: Requirements for ASTM E 108 88
Table 37: Requirements for ASTM E 119 89
Table 38: Requirements for ASTM G 152 89
Table 39: Sample of Exposure Cycles for ASTM G 152 90
Table 40: Requirements for ASTM G 154 91
Table 41: Sample of Exposure Cycles for ASTM G 154 92
Table 42: Requirements for ASTM G 155 93
Table 43: Sample of Exposure Cycles for ASTM G 155 94

Chapter 1: Introduction

Fiber Reinforced Polymers (FRP) are composites made up of a fiber, and a polymer. The fiber and the polymer work together to in structural systems to provide strength. Some common fibers that can be used are glass fiber, carbon fiber, and boron fibers. The fibers may be created in different manners, including woven or chopped strand, and when the fibers are woven, they may be placed at angles in order to achieve certain mechanical properties.

Carbon fiber-reinforced polymers (CFRP) are often used in the aerospace industry because they have strength capacities similar to that of steel but at much lower weight to strength ratio. An example of this would be Boeing's new 747-8, which has been designed with composite wings. However, CFRP's are costly to manufacture. Glass fiber polymers (GFRP) are often used in civil engineering, because the glass fiber costs less to produce. In civil engineering, the most common application for GFRP has been in bridge systems, in which the deck may be made out of a honeycomb composite, or a GFRP sheet may be applied to the bottom of pre-existing concrete beam in order to provide a non-destructive way of strengthening the bridge and extending its life span. GFRP works well with concrete as it is light weight, and water resistant, and therefore can prevent water from entering cracks in the concrete and rusting the steel. However, in recent years, it has also been used as replacements of steel systems in the concrete, for example to replace the steel shear connectors, or steel rebar, thereby reducing the self-weight of the concrete beams. Also, research has been conducted to use GFRP to reinforced concrete columns against blasts in buildings, however, GFRP is not fire resistant, and it emits toxic gases when it burns. Therefore, in order to meet the standards put forth by the International Building Code (IBC), modifications must be made to the GFRP.

This thesis aims to develop a fire-resistant polymer system which satisfies IBC's standards, and therefore is able to be used in buildings. The polymer being used is a polyester isophthalic resin, and the fiber is chopped strand glass fiber. The main concern is the fire resistive properties of the polymers, and how the methods for creating a fire-resistant polymer affect the mechanical properties of the GFRP. Chapter one is an introductory chapter, Chapter two presents a literature review of the IBC showing the requirements which must be fulfilled for the materials. Chapter three is a literature review of methods for creating a fire-resistant GFRP and the effects these methods have on the mechanical properties of the GFRP. Chapter four describes the fire resistant properties of individual additives as well as methods for insulating the GFRP against melting. The optimal additive for fire resistance was selected from the results of these tests and then in Chapter five, the effect this additive had on the GFRP's mechanical properties was tested at various concentrations. Chapter six

summarizes the findings from chapters four and five are summarized and suggestions are made accordingly for further research.

Chapter 2: A Study of the International Building Code

2.1 Introduction

FRP has the ability to be a lightweight building material, however, as of yet, no research has been done to determine methods to alter the resin in the FRP to make it meet the International Building Code's (IBC) standards. It is known that by putting additives into the resin during the mixing process, the resin's fire resistive properties may be improved. However, research has not been done to determine which additive is the optimal additive at achieving the IBC's standards while not affecting the mechanical properties of the FRP. Therefore, this chapter aims at gaining knowledge of what the IBC's standards are for FRP in building applications.

2.2 International Building Code Requirements

In this section, the IBC's requirements for different structural members are investigated. These include the requirements for load bearing members, columns, etc.

2.2.1 Requirements as a Load Bearing Member

2.2.1.1 Fire Resistance based on Types of Construction

In order for the material to be designed according to International Building Code (IBC), it must adhere to the IBC's requirements for fire resistance rating. For structural members these requirements are found in Section 704 of the IBC, for exterior walls these requirements are summarized in Section 705 of the IBC, and for horizontal assemblies these requirements are summarized in Section 711.2 of the IBC, all of these sections state that materials must adhere to the fire resistance rating permitted by the building class. The type of material required for a building type is determined based on the intended use of the building as well as the height of the building. These requirements are defined in Table 503 in Chapter 5 of the IBC. A summary of these limitations can be seen below in Table 1 where UL means unlimited or no requirement.

Table 1: Allowable Building Heights and Stories

Group		Type of Construction								
		Type I		Type II		Type III		Type IV	Type V	
		A	B	A	B	A	B	HT	A	B
	Height (ft)	UL	160	65	55	65	55	65	50	40
A-1	Stories	UL	5	3	2	3	2	3	2	1
A-2		UL	11	3	2	3	2	3	2	1
A-3		UL	11	3	2	3	2	3	2	1
A-4		UL	11	3	2	3	2	3	2	1
A-5		UL	UL	UL	UL	UL	UL	UL	UL	UL
B		UL	11	5	3	5	3	5	3	2
E		UL	5	3	2	3	2	3	1	1
F-1		UL	11	4	2	3	2	4	2	1
F-2		UL	11	5	3	4	3	5	3	2
H-1		1	1	1	1	1	1	1	1	1
H-2		UL	3	2	1	2	1	2	1	1
H-3		UL	6	4	2	4	2	4	2	1
H-4		UL	7	5	3	5	3	5	3	2
H-5		4	4	3	3	3	3	3	3	2
I-1		UL	9	4	3	4	3	4	3	2
I-2		UL	4	2	1	1	NP	1	1	NP
I-3		UL	4	2	1	2	1	2	2	1
I-4		UL	5	3	2	3	2	3	1	1
M		UL	11	4	2	4	2	4	3	1
R-1		UL	11	4	4	4	4	4	3	2
R-2		UL	11	4	4	4	4	4	3	2
R-3		UL	11	4	4	4	4	4	3	3
R-4		UL	11	4	4	4	4	4	3	2
S-1		UL	11	4	2	3	2	4	3	1
S-2		UL	11	5	3	4	3	5	4	2
U		UL	5	4	2	3	2	4	2	1

The group is based on the occupancy type of the building as defined by Section 301 of the IBC. Group A is defined in Section 303 as a building that is used as, “for the gathering of persons for purposes such as civic, social or religious functions; recreation, food or drink consumption or awaiting transportations.” This group is further broken into categories A-1 through A-5 and includes

buildings such as bowling alleys, courthouses, arenas, bleachers, museums, and waiting areas in transportation terminals. Business Group B is defined in Section 304 as a building that is used as, "for office, professional or service-type transactions, including storage of records and accounts." This group includes animal hospitals, kennels and pounds; banks; post offices, etc. Educational Group E is defined in Section 305 as, "the use of a building or structure, or portion thereof, by six or more persons at any one time for educational purposes through the 12th grade." Factory Group F is defined in Section 306 as, "the use of a building or structure or a portion thereof, for assembling, disassembling, fabricating, finishing, manufacturing, packaging, repair or processing operations that are not classified as Group H hazardous or Group S storage occupancy." This group is further broken down into F-1 and F-2 and includes such buildings as bakeries and aircraft manufacturing and are used to store such items as bicycles, clothing, musical instruments, etc. High-Hazard group H is defined in Section 307 as, "the use of a building or structure, or a portion thereof that involves the manufacturing, processing, generation or storage of materials that constitute a physical or health hazard in quantities in excess of those allowed in control areas based on the maximum allowable quantities limits for control areas." High-Hazard group H is subdivided into subsections from H-1 to H-5 based on the type of hazards stored in the building. Section 308 defines Institutional group I as, "the use of a building or structure, or portion thereof, in which care or supervision is provided to persons who are or are not capable of self-preservation without physical assistance or in which persons are detained for penal or correctional purposes or in which the liberty of occupants is restricted." Group I is divided into I-1 through I-3 based on the type of facility and includes detention centers, alcohol and drug centers, group homes, and so on. Section 309 defines Mercantile group M as, "the use of a building or structure, or portion thereof, for the display and sale of merchandise and involves stocks of goods, wares or merchandise incidental to such purposes and accessible to the public." This group includes department stores, drug stores, markets, motor fuel-dispensing facilities, retail or wholesale stores, and sales rooms. Residential group R is defined in Section 310 as, "the use of a building or structure, or portion thereof, for sleeping purposes when not classified as an Institutional group I or when not regulated by the International Residence Code." Further classification of this group is broken down into R-1, R-2, R-3, and R-4 and includes boarding houses, hotels, monasteries, apartment houses, group homes, etc. Storage group S is defined in Section 311 as, "the use of a building or structure, or portion thereof, for storage that is not classified as hazardous occupancy." This group is further broken down into S-1, S-2 and contains buildings that are used to store low and moderately hazardous materials such as furniture, glues, lumber, asbestos, gypsum board, meats and so on. Lastly, Utility and Miscellaneous group U is defined in

Section 312 as, “Buildings and structures of an accessory character and miscellaneous structures not classified in any specific occupancy.” This includes things such as barns, agricultural buildings, carports, tanks and towers.

In order to design a material with the appropriate fire resistance of the materials, Sections 602.2-602.3 of the IBC were referenced which defines five types of construction, each with fire requirements for a Material A and a Material B. These material categories are the same as those from Table 1 and Table 2. Construction types I and II are defined as, “those types of construction in which the building elements listed in Table 601 (Table 2) are of noncombustible materials.” Construction type III is, “that type of construction in which the exterior walls are of noncombustible materials and the interior building elements are of any material permitted by this code.” Construction type IV is heavy timber construction and a Construction type V is, “that type of construction which the structural elements, exterior walls, and interior walls are of any materials permitted by this code.” The required fire-resistance rating for each type of construction is defined below in Table 2 for building elements.

Table 2: Fire-Resistance Rating Requirements for Building Elements

Building Element	Type I		Type II		Type III		Type IV	Type V	
	A	B	A	B	A	B	HT	A	B
Primary Structural Frame	3hr	2 hr	1hr	0hr	1hr	0hr	HT	1hr	0hr
Bearing Walls Exterior	3hr	2 hr	1hr	0hr	2 hr	2 hr	2 hr	1hr	0hr
Interior	3hr	2 hr	1hr	0hr	1hr	0hr	1/HT	1hr	0hr
Roof construction	1.5hr	1hr	1hr	0hr	1hr	0hr	HT	1hr	0hr

The fire resistance rating of the material is to be determined in accordance with ASTM E 119 as defined in Section 703.2 of the IBC.

Section 711.3 also states that for horizontal assemblies separating separate dwelling or sleeping units, the minimum fire resistance rating is defined as one hour.

2.2.1.2 Requirements of Roof Assemblies

The requirements for roof assemblies are defined in Sections 1507 and 1508. These required testing standards are shown below in Table 3, and the standards for each of these tests may be found in the Appendix.

Table 3: Material Testing Standards

Type	IBC Section	Material Name	Testing Standard
Built-up roofs	1507.10.2	Thermoplastics used in roofing applications	ASTM D 5665, ASTM D 5726
Thermoset single-ply roofs	1507.12.2	Thermoset single-ply roofs coverings	ASTM D 4637, ASTM D 5019 or CGSB 37-GP-52M
Thermoplastic single-ply roofing	1507.13.2	Thermoplastic single-ply roofing coverings	ASTM D4434, D6754, D6878 or CGSBB CAN/CGSB27-54
Sprayed polyurethane foam roofing	1507.14.2	Sprayed polyurethane foam roofing	Comply with Type III or Type IV as defined in ASTM C 1029

Where a built-up roof is defined as in section 202 as, “two or more layers of felt cemented together and surfaced with a cap sheet, mineral aggregate, smooth coating or similar surfacing material,” thermoset single-ply roofs are defined as, “a plastic material that is capable of being changed into a substantially nonreformable product when cured,” thermoplastic is defined as, “a plastic material that is capable of being repeatedly softened by increase of temperature and hardened by decrease of temperature,” and sprayed fire-resistant materials are defined as, “cementitious or fibrous materials that are sprayed to provide fire resistant protection of the substrates.” Since the material being developed is not a single-ply system, the requirements for thermoset and thermoplastic single-ply roofing are not applicable.

In addition, according to IBC Section 1507.14.4, foam plastic materials and insulation are to comply with IBC Chapter 26. A summary of this information can be found in Section 2.3.2 of this thesis. Also, according to IBC Section 1507.16.1, the fire resistance of the materials must comply with requirements outlined above in Table 2.

Lastly, “The minimum roof covering installed on buildings must comply with Table 1505.1 based on the type of construction of the building.” These requirements are summarized in Table 4 below

where the types of construction are as defined by the fire resistance of a material based on Table 2, and the requirements are explained below in Table 5. Class A is the highest achievable category for materials with a "severe" effective fire test exposure, meaning that it is the materials which can provide the best fire resistance. The requirements to meet Class C are the least restrictive with only a "light" effective fire test exposure.

Table 4: Minimum Roof Covering Classification for Types of Construction

IA	IB	IIA	IIB	IIIA	IIIB	IV	VA	VB
B	B	B	C	B	C	B	B	C

In order to fulfill the requirements for high rise buildings, the materials in Chapter 4 will be tested to ensure that they withstand the correct effective fire test exposure, according to ASTM E 108 and UL 790. These tests determine which class the material belongs to, Class A, Class B, or Class C, with Class A being the most durable and safe material, and Class C being the minimum material requirements. A summary for these categories can be found below in Table 5.

Table 5: Roofing Materials Classification

Class	**Effective fire test exposure**	**Test**	**Acceptable Building Types**	**Additions**
A	Severe	ASTM E 108 or UL 790	All	Includes exposed concrete roof deck
B	Moderate	ASTM E 108 or UL 790	not specified	None
C	Light	ASTM E 108 or UL 790	not specified	None

2.3 FRP as an Interior Finish

Foam plastic cores may be used in conjunction with FRP if the foam plastic adheres to the requirements provided in IBC Chapters 8 and 26. As defined by Section 803.9, interior walls and ceiling walls will be designed to have a flame spread corresponding to those in Table 6 based on location and group.

Table 6: Interior Wall and Ceiling Finish Requirements by Occupancy

Group	Sprinklered			Non Sprinklered		
	Interior exit stairways, interior exit ramps and exit passageways	Corridors and enclosure for exit access stairways and exit access ramps	Rooms and enclosed spaces	Interior exit stairways, interior exit ramps and exit passageways	Corridors and enclosure for exit access stairways and exit access ramps	Rooms and enclosed spaces
A-1, A-2	B	B	C	A	A	B
A-3, A-4, A-5	B	B	C	A	A	B
B, E, M, R-1	B	C	C	A	B	C
R-4	B	C	C	A	B	B
F	C	C	C	B	C	C
H	B	B	C	A	A	B
I-1	B	C	C	A	B	B
I-2	B	B	B	A	A	B
I-3	A	A	C	A	A	B
I-4	B	B	B	A	A	B
R-2	C	C	C	B	B	C
R-3	C	C	C	C	C	C
S	C	C	C	B	B	C
U	No Restrictions			No Restrictions		

Where the group or type of occupancy is defined above in 2.2.1.1 and the material class is defined above in Table 6.

In addition, the materials are to be classified according to their Flame Spread Index, which is different from Flame Spread, and Smoke-development index as defined by chapter 8 of the IBC as, “A comparative measure, expressed as a dimensionless number, derived from visual measurements of the spread of flame versus time for a material,” and “A comparative measure expressed as a dimensionless number, derived from measurements of smoke obscuration versus time for a material,” respectively. Both of these are to be determined through testing according to ASTM E 84 or UL 723. Both the flame-spread requirements and smoke development requirements are summarized below in Table 7.

Table 7: Material Classification

Class	Flame spread index	Test	Smoke Spread Index	Test
A	0-25	ASTM E 84 or UL 723	0-450	ASTM E 84
B	26-75		0-450	
C	76-200		0-450	

2.3.1 FRP as a Roofing Material

2.3.1.1 Accelerated Weathering Tests

The requirements for accelerated weathering tests of a roofing system are defined by IBC section 1504.6 which states that "Roof coverings installed on low-slope roofs in accordance with section 1507 shall demonstrate physical integrity over the working life of the roof based upon 2,000 hours of exposure to accelerated weathering tests conducted in accordance with ASTM G 152, ASTM G 155, or ASTM G 154." In addition, the materials that are subject to a cyclical flexural response due to wind load are not to demonstrate significant loss of tensile strength for unreinforced membranes or breaking strength for reinforced membranes.

2.3.1.2 Water Resistance

Water leakage requirements for an FRP roofing system are defined by section 4.5 of FM Approvals (2010). Section 4.5 states that water leakage must be tested in accordance with ASTM D7281. The material will be deemed acceptable if there are, "no signs of water leakage during the 7 day period. In addition, there shall be no signs of water leakage during, or after, the pressure cycles."

2.3.1.3 Combustion Test

The combustion requirements for materials are defined in the IBC Section 1505.1 which states that materials must be tested in accordance with ASTM E 108. The requirements for combustion are expanded on by FM Approvals (2010). FM Approvals separates roofing systems into above the roof deck and below the roof deck as summarized in the following sections.

2.3.1.3.1 Above the Roof Deck

The materials above the roofing must be tested in accordance with ASTM E108. The tests are to include flame spread, intermittent flame and burning brand as applicable. For each class of decking

type, the requirements are summarized below in Table 8, which are the FM requirements, but they correspond to the requirements in ASTM E108 as well.

Table 8: FM Approvals Flame Spread Requirements for Above the Roof Deck

Material	Flame Spread (in)
A	≤72
B	72< FS ≤ 92
C	92< FS ≤ 156

The different classes of materials are to be used in accordance with the type of construction, as defined above in Table 2 and Table 4, and according to the material classification based on the height of the building, occupancy of the building, and the material location in the building as defined by Table 1 and Table 6.

In addition to these requirements, FM Approvals also states that, "There shall be no excessive lateral flame spread of which is defined as flames extending to the two lateral edges of the exposed roof covering or coating beyond 12 in from the ignition source." Also, no glowing or flaming brands may be blown or falling off of the roofing system may be blown that continue to glow after reaching the floor. Lastly, no particles of the roofing system may continue to glow after falling to and reaching the ground.

The requirements for intermittent spread of flame and burning brand tests for classes A, B or C state that 1. "There shall be no portion of the roof covering material blown or falling off of the test deck in the form of flaming or glowing brands that continue to glow after reaching to floor," 2. "There shall be no exposure of the deck or sustained flaming on the underside of the deck," 3. "There shall be no potion of the roof deck that fall in the form of particles that continue to glow after reaching the floor."

2.3.1.3.2 Below the Roof Deck

The tests for the below deck roofing materials must be conducted in accordance with Test Procedure, *FM Approvals Construction Materials Calorimeter*, FM Approvals, LLC. When materials are exposed to the Construction Materials Calorimeter test, they must have fuel contribution rates lower than the rates summarized in Table 9.

Table 9: Requirements for Calorimeter Test

Time Interval	Maximum Fuel Contribution Rate	
min	$Btu/ft^2/min$	kW/m^2
3	410	77.6
5	390	73.8
10	360	68.1
Avg. 30 min	285	54

In addition to the maximum fuel contribution rate, while performing the test, no flaming particles from the sample may drop into the furnace, and also there shall be no uncontrolled flaming on the exterior surface of the sample.

2.3.2 Requirements for Foam Insulation and FRP

The requirements for foam insulation and FRP are defined in Chapter 26 of the IBC. Chapter 26 defines the required fire resistance and smoke requirements.

2.3.2.1 FRP

The requirements for FRP as a building material are defined in Section 2612 of the IBC, and the use of FRP for exterior use is defined in Section 2612.5 of the IBC. Section 2612.5 states that, "FRP shall be permitted to be installed on the exterior walls of buildings of any type of construction when such polymers meet the requirements of Section 2603.5. Fireblocking shall be installed in accordance with Section 718. There are two exceptions which make the FRP not need to meet the requirements of Section 2603.5. The first states that if the FRP does not exceed 20 percent of the area of the specific wall, the FRP has a flame spread index less than 25, fireblocking in accordance with Section 718.2.6 is installed, and the FRP is installed directly to a noncombustible material; examples of this are gypsum or concrete. The second exception is for buildings that are 40 ft or less above grade. Since the material is being designed for applications in high rise buildings, this exception does not apply. Section 718.2.6 states that fireblocking is to be installed at maximum intervals of 20 feet in either direction so that there is no concealed space exceeding 100 ft^2 between fireblocking. Fireblocking according to 718.2.6 is not required if the exterior wall covering is installed on noncombustible framing, or if the exterior wall covering is tested in accordance with NFPA 285. The last requirement for FRP is self-ignition temperature, which is defined by section 2605.2 of the IBC which states that the self-ignition temperature of an FRP not be greater than 650 degrees Fahrenheit, as tested according to ASTM D 1929.

2.3.2.1 Foam Plastic Insulation

The requirements of foam plastic insulation are defined in Section 2603 of the IBC. The requirements for the surface burning characteristics are defined by the flame spread and smoke developed index requirements as specified in IBC Section 2603.3. These requirements are summarized below in Table 10. The exception to Table 10 is that if the foam plastic insulation is part of a Class A, B, or C roofing system as tested by FM 4450 or UL 1256 in which case the smoke development index is unlimited.

Table 10: Foam Plastic Insulation Flame Spread Index and Smoke Development Index

Flame Spread Index	Smoke Development Index	Test	Exception (Roofing System Class A, B, C)	Test
≤ 75	≤ 450	ASTM E84 or UL 723	Unlimited	FM 4450 or UL 1256

In addition, foam plastic insulation which has a thickness greater than four inches is required to be tested at a minimum thickness of four inches and must have the same flame spread index and smoke development index as shown in Table 10.

For a foam plastic insulation, the use and design of a thermal barrier is defined by IBC section 2603.4 which states that, "foam plastic shall be separated from the interior of a building by an approved thermal barrier of ½ inch gypsum wallboard or material that is tested in accordance with and meets the acceptance criteria of both the Temperature Transmission Fire Test and the Integrity Fire Test of NFPA 275. However, according to IBC Section 2604.1.5 a thermal barrier is not required if the foam plastic insulation is part of a Class A, B, or C roofing system. In addition, according to Section 2603.6 of the IBC, foam plastic insulation is permitted for use in a roofing system as outlined above if the roofing system with the plastic insulation is a Class A, B, or C roofing system where tested in accordance to ASTM E 108 or UL 790. Because of this requirement, a thermal barrier is not required of the roofing system.

2.4 Summary

In Table 11 are presented the tests required by the IBC. The details for each of the ASTM and UL test that is mentioned in Table 11 may be found in the Appendix.

Table 11: Summary of Required Testing Method

Property/Material Testing:	Test Method:	
	ASTM	Other
Fire resistance Rating	ASTM E 119	
Built-up roofs	ASTM D 5665, ASTM D 5726	
Sprayed polyurethane foam roofing	ASTM C 1029	
Flame Spread Index	ASTM E 84	UL 723
Smoke development Index		
Weathering Test	ASTM G 152, ASTM G 155, or ASTM G 154	
Water Resistance	ASTM D 7281	
Combustion Test	ASTM E 108	
Above Roof Deck	ASTM E 108	
Foam Plastic	ASTM E 84	UL 723
FRP Roofing System	ASTM E 108	UL 790
Self-Ignition Temperature	ASTM D 1929	

Chapter 3: A Literature Review of FRP and Polystyrene as Building Materials

3.1 Introduction

In order to determine previous methods for enhancing the fire resistant properties in FRP, a literature review was done on research which may benefit from a fire resistant FRP (Section 3.2), and on methods for creating a more fire resistant system (Section 3.3).

3.2 Structural

Numerous studies have been performed to determine the behavior of FRP for building applications. Both carbon fiber reinforced polymer (CFRP) and glass fiber reinforced polymer (GFRP) have been investigated for use in structural systems. Chowdury, et al. (2008) looked into the remaining structural strength in building systems after a fire event. They studied reinforced concrete beams which had been strengthened with CFRP sheets flexurally, and found that CFRP was able to retain structural integrity after a fire event. However, GFRP is being used in order to control the cost of the roof panels, therefore the remaining studies are on GFRP in structural systems. Studies have been performed to compare steel reinforcement to GFRP reinforcement in concrete columns and beams. In addition, externally bonding FRP to different building materials has been investigated.

Mukhopadhyaya, et al. (1998) studied whether FRP could be used in conjunction with concrete. They found that there was a maximum thickness of the FRP, but that it could perform well as a flexural reinforcement for concrete beams.

Much research has been done on columns, with Herig and Motavalli (2012) studying the axial behavior of reinforced concrete beams which had been externally strengthened with either lightweight concrete or with unbounded GFRP wrapping i.e., there was no adhesive or other connecting mechanism between the GFRP wrapping and the concrete. They found that using GFRP for strengthening concrete columns axially was a promising method, but needed more research. Pantelides, et al. (2012) investigated the performance of concrete panels reinforced with synthetic fibers, mild steel, and GFRP when subjected to blasts. They found that GFRP and steel worked well for blast resistance depending on the anchoring type; however, steel was a more ductile material.

Mirmiran, et al. (1999) studied the effects that wrapping hybrid concrete beam-columns with FRP would have on the strength and ductility of the beams. This test focused on the short-term static loading. The beam-columns were tested using various axial and transverse load cases, and it was found that Euler-Bernoulli beam theory was applicable, and that the FRP wrapped concrete columns

were stronger than concrete columns with no stiffeners, and that failure was a ductile failure and therefore provided ample warning.

Studies have also been completed to determine the effects that GFRP has on the strength of wood when bonded to the surface of the wood. Davalos, et al. (2000) investigated the effects on durability and shear strength by testing according to ASTM D 2559 and D 905 to check the bond strength between the FRP and the wood under both wet and dry conditions. They studied the bond strengths of different resins, and found that ASTM D 2559 was sufficient for predicting the delamination, but that performance evaluations tests do not provide enough information to predict the specific failure mode for delamination.

After several tests were performed for this experiment, it was found that it was ideal to include gypsum into the system to provide a heat shield for the FRP. In so doing, the FRP was not allowed to reach its heat defection temperature, nor was the foam allowed to reach its melting temperature. This process is discussed more in Chapter 4; however, because of this, it was necessary to determine the type of reaction between gypsum dry wall and GFRP. Reyes, et al. (2009) investigated the effect of strengthening gypsum with FRP in a shear wall system. The aim of this study was to determine the system's performance in an earthquake, and it was found that this system could perform with similar results to that of a properly designed plywood shear wall. Therefore, gypsum and FRP do have potential to perform well in conjunction with each other.

Pantelides, et al. (2012) investigated the possibility of using a hybrid GFRP/steel concrete panel in order to develop composite action between a concrete-foam composite. From their tests they found that the FRP connecting system was sufficient at transferring the shear between the two concrete withes.

Belzer, et al. (2013) studied the degree of composite action (DCA) for different levels of bonding between concrete and GFRP by testing a concrete filled GFRP tube in four-point bending. The results from this test were compared to a concrete filled steel tube and a concrete filled GFRP tube with CFRP tension flanges. The GFRP tube tested by Belzer, et al. (2013) is similar to the top of a roofing system as there will be composite action between the top layer of GFRP and concrete. They found that the DCA depends on the level of concrete-to-tube bonding. However, they were able to achieve full composite action, and therefore failure was predictable.

Lastly, limited research has been performed to determine how GFRP performs structurally after a fire has occurred. Foster and Bisby (2008) tested the bond strength between FRP and concrete as

well as FRP to FRP via testing the ultimate tensile strength, elastic modulus, and failure strain at a range of temperatures. It was found that the strength of the bond was influenced by the bond strength of the adhesive used to bond the FRP to the concrete. The study also found that GFRP's bond strength begins to dramatically decrease after 300^0C likely due to the melting temperature of the polymer being surpassed.

From these, it can be seen that FRP is applicable in use in buildings; however, for this to happen they must be altered in order to meet IBC standards. Various methods for achieving this are summarized in Section 3.3.

3.3 Materials

In addition to looking at the structural performance of FRP in structural applications, methods for altering resins to improve the fire resistant properties of the resin were investigated. Also, methods to surface treat the polystyrene were investigated.

One of the additives that were investigated was rice hull ash (RHA). Due to the high silica content in the RHA, it was theorized that RHA could be a good fire retardant when added to a polymer system. Chand, et al., (1987) investigated the implications of using RHA as an additive to polyester composites. The RHA was added in to the resin using volume fractions and after curing, tensile and impact strength was measured. Because RHA is weak in tension, it was found that it also decreased the tensile strength of the system. Also it was found that RHA decreases the impact strength of the system using the IZOD impact test. Unfortunately, when RHA is generated at low temperatures it has a black color, which absorbs heat and therefore is not conducive to utilization in green environments. Chakraverty, et al. (1988) aimed at completing the following objectives through their research: 1. to determine the effects of various acid treatments on process of removing metallic impurities from the RHA, and 2. to determine the effects of acid treatments and different furnace temperatures on the time required to obtain completely white RHA. While it was found that the acid wash did not affect the silica structure of the RHA, it also did not affect the time for complete combustion of the RHA in order to produce a white silica product.

Another additive that was investigated was nanoclay (NC). Nazare, et al. (2006) investigated the use of NC in polyester resin to reduce smoke generation and improve the fire resistance of the system. They found that the addition of NC helps reduce the flammability because the dispersion of clay in the polymeric matrices produce a nanocomposite structure which allows for reduced flammability as well as improved mechanical properties, in addition the NC forms a char layer which helps insulate

the system. It was noticed that for higher clay concentrations (>5% clay) in combination with flame retardants, the crosslinking reaction, or the development of the nanocomposite structure in the nanoclays, was noticeably slower and therefore it was not able to form a complete crosslinked barrier. In addition to this problem, the resin also became more plastic and had an increased cure time when the clay concentrations were high. From using the X-ray diffraction, it was found that little to no nanocomposite was formed. From the cone calorimetry test, it was found that the time to ignition improved by 102 seconds. Therefore, nanoclay is a viable option for fire resistance in the GFRP.

Wu, et al. (2007) looked into using NC in conjunction with expoxy adhesives to provide fire resistant properties for the epoxy. This study investigated the various flame spread tests and high-temperature exposure tests. They found that NC can greatly improve the flame retardancy of epoxy systems at filling levels of 2%-3%. They also found that NC which was distributed into the epoxy using a mixer was better at improving fire properties than NC which was not.

Intumescents were also studied by Kandola, et al. (2002) to see how they changed how polyester resin-composites burned. Intumescents are often found in paints and ceramics, and therefore may be incorporated into a building system. They found that intumescents significantly decrease the flaming behavior of the resins tested, however, the decrease is not as significant as was expected. Also, they found that the intumescents did not help the structural integrity of the composite; therefore they suggest that intumescents be used as a protective coating on thick laminates.

Dholakiay (2009) investigated the effects the following four different additives had on resins. These were: 1. Hydroxyapatite or calcium phosphate, 2. zinc borate, 3. class C fly ash, and 4. Antimony trioxide. They were tested for their fire resistance using LOI using ASTM D2863, TGA and IR spectroscopy. The materials are considered self-extinguishing if the LOI is greater than 26, and all of the composites tested had an LOI in the range of 25-26. Therefore, they are self-extinguishing. It was also found that as the amount of fillers increases, so does the fire resistance of the composite. From this, it was shown that while fly ash is a good additive, hydroxyapatite and zinc borate are better for increasing LOI. From the TGA, it was found that composites containing filler have a better thermal stability. Mechanical properties were tested for the samples using Rockwell hardness test and flexural strength tests. From these tests it was found that the mechanical properties increase as the filler content increases. The exception to this was for antimony trioxide and fly ash.

Additionally, the toxicity of the chemicals release during a fire event must be investigated. Manfredi, et al. (2006) compared the fire resistance and smoke evolution of different natural composites and

glass fiber composites containing the same matrix. The natural fibers used were sisal, jute and flax. The glass composites showed more fire resistance, however, it had a higher emission of CO and CO_2.

Another concern in the system is the foam retaining structural integrity in the event of a fire. Laufer, et al. (2013) studied effects of layer-by-layer (LbL) assembly on fire resistance of foam. LbL is deposition technique that grows thin films through dipping the materials in oppositely charge polyelectrolytes and nanoparticles. This protects the polymer by forming an inorganic particle layer or intumescent char. In this study, a flame retardant nanocoating was prepared by pairing chitosan with poly sodium salt. This coating works because as it degrades, it releases fire-retardant gases which dilute the oxygen and starve the flame. The fire resistance was initially screened by holding a butane torch to the foam's surface for 10 seconds. By doing this, it was found that the foam containing no surface treatment was subjected to immediate melting, however, as the surface treatment thickness increased, the structural integrity was maintained more. In fact, the thickest surface treatment (10BL) melted very little and maintained the majority of its structure.

Bourbigot, et al. (2009) tested whether adding polyhedral oligomeric silsesquioxane (POSS) to thermoplastic polyurethane (TPU) could improve the fire resistive properties of the TPU. They tested the TPU using LOI, and FTT. They also did a thermogravimetric analysis, a solid state NMR, and determined the swelling and heat gradient of the samples. They found that with the POSS added, the system created a ceramified char composed of a silicon network which limits the heat and mass transfer, and leads to improved thermal behavior of the TPU.

Aziz, et al. (2005) investigated how modifying polyester resins with additives would change the mechanical properties, glass transition temperature, fracture surface, and bond performance of the systems. They found that adding kenaf – a plant fiber – did improve the mechanical behavior of the composites.

Alpolic Materials (2011) developed a roof panel. Alpolic Materials' material was developed in order to strengthen reinforced concrete beams called Alpolic/fr Composite Fire Resistive Metal Panels. Alpolic's material was tested for fire resistance according to ASTM E84, ASTM E119, and ASTM E1929. The material was also tested for sound insulation according to ASTM E413 and for water penetration according to ASTM E331.

From this it may be seen that by adding various additives to a resin system the fire resistance of the system may be increased. Therefore, for this thesis, in order to achieve the required fire resistance, additives will be added to the system.

3.4 Conclusion

From the literature review, it can be seen that while studies have been done on the using GFRP in building applications, and the effects that different fillers have on the fire resistance properties of resins in general, additional research is needed to determine fillers which are readily available for building systems. Therefore, the aim of Chapter 3 is to determine the best additive in isophthalic polyester resin and then to analyze the effects of that resin and additive on the whole system. The aim of Chapter 4 is to determine how the selected additive changes the mechanical properties of the GFRP as the loading of the additive changes.

Chapter 4: Thermodynamic Properties of the FRP and Polystyrene

4.1 Introduction

The first step in developing a fire resistant system is to perform simple tests in order to obtain a basic understanding how different additives affect the fire resistance properties of the composite material. The main goal of this report is to compare the fire resistance provided by adding various additives to the resin which were: alumina trihydrate (ATH), a mixture of boric acid and rice hull ash (BA/RHA), coarse graded gypsum (CG), coarse graded limestone (CLS), a mixture comprised of 60% BA, 20% RHA, 10% limestone, and 10% ATH (Conc), fine graded gypsum (FG), fine graded limestone (FLS), nanoclays (NC), and rice hull ash (RHA). In addition, two controls were created with no additives to the resin, one with 1% MEKP hardener and the other with 5% MEKP hardener.

After the preliminary tests had been completed, the second step in developing a fire resistant system is to determine the ideal amount of different types of additives to create the ideal fire-resistant system. This was completed using a workability test. The additives which were tested for workability were the materials selected for additional testing from the preliminary test.

Lastly, the ideal amounts of additives were used to create samples with fire retardant resins. These resins contain fire resistant properties, and therefore, it is thought that the combination of the special resin with the best fire resistant additives will create a system which will be able to meet the IBC requirements for fire resistance. One fire resistant resin will be tested which is a halogenated polyester resin made by AOC (fr1). The properties for both the control resin and fr1 may be seen below in Table 12.

Table 12: Resin Properties

	Tensile Strength (ksi)	Flexural Strength (ksi)	Heat Disortion Temperature (^{o}C)
Control	7.3	15.3	106
FR1	11	18	96

4.2 Testing (Preliminary ASTM E 108)

4.2.1 Specimen Setup

4.2.1.1 Preliminary Testing

In order to determine how isophthalic polyester resin reacts with separate additives, a flame test was completed using a propane torch. Due to the decreased cure time and no harmful consequences of using 5% MEKP on fire resistance, a resin concentration of 5% MEKP was used in the rest of the samples. For the CLS, FLS, and gypsum systems, six separate samples were made with the amount of additives in the resin varying from 5% to 50%. Four samples were made for the FG varying from 10% to 50% in increments of 10%.Three samples were made for the ATH and the NC varying from 30% to 50% in increments of 10%. For RHA, due to the unworkable nature of the 40% sample, at 50% sample was not created and therefore only samples with 5%, 10%, 20%, 30%, and 40% RHA were created. In addition, at a 40% RHA concentration, there was not enough resin to completely saturate the RHA, and therefore it had a very spongy texture and was not able to soak through the chopped strand mat. After testing the RHA samples, more RHA samples were created in the hopes of creating increased fire resistance. In order to improve the fire resistance, the RHA was mixed together with BA with 50% of each which was then added to the resin system in concentrations of 40 parts per hundred (pph) and 50 pph. The reasoning behind this was the hope that when heat was applied to the sample, the boric acid would melt and mix with the silica in the RHA, allowing it to form a more effective char layer. Lastly, the Conc sample was made at 70 pph. The sample was made at this concentration due to the results from the workability test as described in 4.2.1.2.

The samples were created using one layer of 1.5 oz. chopped strand mat. The chopped strand mat was placed onto paper plates or sheet metal, and resin/additives were added. The resin/additive/MEKP mixture was produced by first measuring the weight of the resin required, then adding the required weight of additives. The additives and the resin were then mixed, after which the MEKP hardener was also mixed into the resin. The resin was then applied to the chopped strand mat on the paper plate. It was then labeled, and the time until initial setting was recorded as can be seen in Table 13. After the resin had cured for 17 hours, the samples cast on the sheet metal or on paper were released by bending the steel away from the composite, and fire testing was conducted. However, the paper did not always debond from the composite correctly and therefore paper remained on the sample after the backing was removed.

Table 13: Time to set for additives

	Time to set (min)								
	% Additive								
	MEKP 1%	60 min	MEKP 5%	25 min					
	5%	10%	20%	30%	40%	50%	40 pph	50 pph	70 pph
ATH	n/a	n/a	n/a	55	40	37	n/a	n/a	n/a
BA/RHA	n/a	n/a	n/a	n/a	n/a	n/a	25	25	n/a
CG	35	20	30	30	20	20	n/a	n/a	n/a
CLS	40	35	20	20	15	15	n/a	n/a	n/a
Conc	n/a	n/a	n/a	n/a	n/a	n/a	n/a	n/a	15
FG	n/a	20	25	22	20	20	n/a	n/a	n/a
FLS	35	20	15	15	15	15	n/a	n/a	n/a
NC	n/a	n/a	n/a	50	60	50	n/a	n/a	n/a
RHA	25	15	20	3	2	n/a	n/a	n/a	n/a

In order to test the samples, samples were heated using a propane torch by holding the sample with forceps in the blue section of the flame for ten seconds. The flame was then removed, and the samples were allowed to self-extinguish. The time to ignition, the time to self-extinguish, the smoke color, and the smoke quantity were recorded and are reported in Table 14 and Table 15. Since, as mentioned above, the paper backing bonded to the composite, the residual paper had a chance of catching fire, and skewing the results. If this happened, a star was added besides the results. In addition, pictures were taken before and after to show to burn characteristics of the sample.

4.2.1.2 Workability Limit Test Set Up

Workability limits were found for ATH 202 (ATH1), ATH 802 (ATH2), and Conc in both the special resin and the standard resin and FG was tested with the special resin. FG was only tested for the special resin because the preliminary tests showed that the ideal amount of additives to add to the resin system was 40% of the system. Preparation for the workability limit was completed by weighing out the initial amount of additives that would be added to the resin system. The initial amount for the ATH1 and the ATH2 for both resin systems was 4 g, for the Conc it was 2 g, and for the FG in the special resin it was 30 g. After the initial amount of additives had been weighted out, 10 1 g samples were weighed out for each additive. After this was completed, 10 g of the appropriate

resin was weighed out, and the initial amount of the respective additive was stirred in vigorously, avoiding the formation of air bubbles. The sample's workability was then rated on a scale of 0-10, 10 being very workable and 0 being not workable. The workability was determined by the resin/additives ability to spread as well as its ability to run. After the initial amount's workability was recorded, the workability was tested in 1 g increments.

4.2.1.3 Special Resin Samples

The samples with the special resin were created for the ATH1, ATH2, FG, and the Conc using the same approach as before, but only with the optimal amount of additives, as found from the workability test. The sample for the CG was created by applying CG over the entire surface of the fiberglass so that it is tightly packed, and then pouring the resin with the MEKP over the CG, making sure that the resin completely soaked through the fiberglass. The special resin required more time to cure, and therefore these samples were tested after 48 hours of curing instead of 17 hours.

4.3 Results

4.3.1 Fire Results

After testing the CG, CLS, FLS and RHA, it was found that the paper backing could not be removed from the samples. Due to this, the fire resistance for these samples was skewed because the paper backing sometimes caught fire as well and then the system was unable to self-extinguish. Therefore, the rest of the resin/additive mixtures were cast on flexible sheet metal and then released from the sheet metal before testing. The tests which were affected by the paper backing catching fire can be seen starred in Table 14.

Table 14: Results from flame test

Additive	% Additive	Time to ignition (sec)	Time to self-extinguish (sec)
Controls	1% MEKP	1	2
	5% MEKP	1	2
ATH	25%	3	6
	40%	5	4
	50%	6	2
BA/RHA	40 pph	4	3
	50 pph	2	(fire consumed sample)
Coarse Gypsum	5%	3	3
	10%	5	1
	20%	4	0.5
	30%	5	0
	40%	6	0
	50%	15	0
Coarse Limestone	5%	2	3
	10%	3	12*
	20%	3	4
	30%	2	2
	40%	3	5
	50%	5	4
Conc	70 pph	15	0
Fine Gypsum	10%	3	2
	20%	0	n/a
	30%	5	2
	40%	5	2
	50%	6	3
Fine Limestone	5%	Instant	20
	10%	Instant	9
	20%	1	2
	30%	3	2
	40%	2	2
	50%	2	2
NC	30%	2	(fire consumed sample)
	40%	2	28
	50%	2	0*

Table 13: Continued

Additive	% Additive	Time to ignition (sec)	Time to self-extinguish (sec)
Rice Hull Ash	5%	4	2
	10%	3	10*
	20%	3	5
	30%	3	3
	40%	3	2

*Indicates that the paper backing caught fire

4.3.1.1 ATH

ATH is currently the standard additive used for improving fire resistance, and it was shown to work very well above at or above 25% ATH, with 50% ATH performing the best of the samples. The time to ignition for the 50% ATH was 6 seconds, which is a 4 second improvement from the controls. Unfortunately, the time to self-extinguish, which is two seconds, is equal to that of the controls. However, from Figure 1, it is clear that as the percent of additives increases, the time to ignition increases, and the time to self-extinguish decreases. This is true until the resin/additive mixture is no longer workable, at which time the fire resistance is compromised. Because of this, it can be concluded that as long as the resin/additive mixture remains workable, the time to ignition will continue to increase, and the time to self-extinguish will continue to decrease at 60% ATH and 70% ATH.

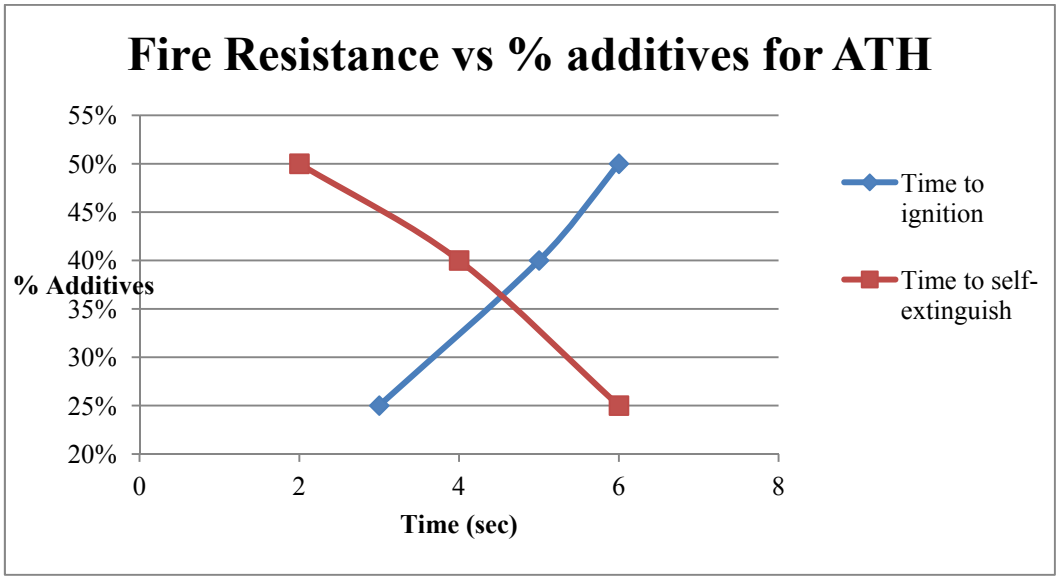

Figure 1: Fire resistance vs. % Additives

4.3.1.2 BA/RHA

The addition of BA to the RHA did not improve the fire resistance of the samples. In fact, for a concentration of 50 pph, the fire resistance was non-existent and the sample was consumed and had to be dunked in water to extinguish the fire. For the 40 pph sample, the time to ignition increased from the control from 1 second to 4 seconds, but the time to self-extinguish increased from 2 seconds to 3 seconds. Therefore, the BA/RHA mixture is not a viable way to provide fire-resistance.

4.3.1.3 CG

From the Table 14, it can be seen that the gypsum additive at a 50% concentration provides the best fire resistance. This sample did not catch fire during the 10 seconds that the propane torch was applied to it, and therefore had no need to self-extinguish. To test the time to ignition for the 50% gypsum sample, the propane torch was applied to the surface of the sample until flames were visible and then removed. In this case, the sample required 15 seconds to ignite. The flame melted through the resin to the paper backing, and the paper was ignited making the sample unable to self-extinguish. When compared to the controls, all of the samples cured more rapidly and had a higher time to self-ignition. In addition, the samples greater than or equal to10% of the system gypsum also self-extinguished more rapidly. However, for the systems greater than or equal to 30%, the time to self-extinguish was near instantaneous once the flame was removed. The gypsum worked so well because the gypsum began to melt upon application of the flame and provided an insulating layer.

4.3.1.4 CLS

While the CLS was effective at delaying the ignition time at least one second the 30% ATH or higher, and 4 seconds for the 50% CLS, it was not effective at self-extinguishing. The self-extinguish time for the controls is 2 seconds for both, and the shortest time for the CLS to self-extinguish was 3 seconds. This may be because the limestone did not melt under the heat, and therefore there were gaps that allowed the heat to ignite the resins and the paper backing.

4.3.1.5 Conc

The result for the Conc at 70 pph is very comparable to the results of the CG. Like the 50% CG sample, the Conc sample also did not ignite after 10 seconds, and therefore did not have a self-extinguish time. Because of this, the propane torch was applied until the sample ignited, and then time to self-extinguish was measured. The time to ignite was 15 seconds, as for the CG. However, while the CG had to be extinguished with water after it was ignited, the Concr self-extinguished after 6 seconds. Therefore, this material is a viable option for the flame test.

4.3.1.6 FG

At 20% FG the sample ignited instantly and was unable to self-extinguish. However, it seems that there may have been something wrong with the sample. All of the other samples performed very well, with 10% providing a 1 second improvement from the control for ignition time. At 50% FG, the sample improved from the control by 5 seconds to the ignition time. However, the 50%'s self-extinguish time was up one second longer. However, at 50%, the FG was not workable, which may explain the 1 second increase in time to self-extinguish from the control as time to self-extinguish will continue to increase until workability has been compromised, and then it will decrease. Therefore, it can that 40% FG was the most efficient at fire resistance which has an increase of 4 seconds from the control and no increase or decrease in self-extinguish time from the control.

4.3.1.7 FLS

The FLS provided the worst fire protection of all the systems. Both the 5% and 10% FLS had an instantaneous ignition time. Also, the time to self-extinguish increased from 2 seconds for the controls to 20 seconds for the 5% and 9 seconds for the 10%. The self-extinguish time for the rest of the FLS samples was equal to that of the control sample. However, the ignition time did increase with higher amounts of limestone additive. The best ignition time for the FLS was 30% limestone with an ignition time of 3 seconds.

4.3.1.8 NC

From the results in Table 14, it can be seen that for NC with less than 50% did not perform well. The 40% sample has a one second increase in time of ignition, but also had a self-extinguished time of 28 seconds, which was a 26 second increase from the controls. However, the 50% NC sample ignited after 2 seconds, but then put itself out while the propane torch was still being applied, putting out the propane torch at the same time. Unfortunately, the 50% NC/resin mixture was unworkable pre-curing, and was unable to completely soak through the fiberglass. Because of this, the NC was rejected for further testing.

4.3.1.9 RHA

The RHA preformed the best at 5%. At this amount of RHA added to the resin, the ignition time was increased from one second for the controls to 4 seconds. However, the time to self-extinguish was unchanged from the controls.

4.3.2 Smoke Results

The smoke development was measured from videos that were taken of the tests. If the smoke was black, this indicated that the paper backing was potentially burning or that there were noxious fumes being released. In addition, the amount of smoke released was also quantified from low to very high. The results for each sample are summarized in Table 15.

Table 15: Results from Smoke Test

Additive	**% Additive**	**Smoke Color**	**Smoke Development**	Additive	**% Additive**	**Smoke Color**	**Smoke Development**
Controls	1% MEKP	Black	Medium	Conc	70 pph	None	None
	5% MEKP	Black	High	Fine Gypsum	10%	Black and White	Low
ATH	30%	Black	High		20%	Black	Very High
	40%	White	Low		30%	White	Low
	50%	White	Low		40%	White	Low
BA/RHA	40 pph	White	Medium		50%	White	Low
	50 pph	Black	High	Fine Limestone	5%	Black and White	Low
Coarse Gypsum	5%	Black	Very High		10%	Black and White	Medium
	10%	White	Medium		20%	White	Medium
	20%	White	Medium		30%	White	Low
	30%	White	Low		40%	White	Medium
	40%	White	Low		50%	White	High
	50%	None	None	NC	30%	Black and White	Very High
Coarse Limestone	5%	White	High		40%	Black	Very High
	10%	Black	High		50%	White	Medium
	20%	Black	High	Rice Hull Ash	5%	White	Medium
	30%	Black	Low		10%	White	High
	40%	White	Low		20%	Black	High
	50%	White	Low		30%	Black	High
					40%	White	High

4.3.2.1 ATH

With 30% ATH added to the resin, the samples did not perform well, with a black smoke color and high smoke quantity. However, for 40% and 50% ATH added, the smoke was white and the quantity

of smoke produced was low. Because of these smoke results combined with the results from the fire resistance, ATH was selected for further testing.

4.3.2.2 BA/RHA

From Table 15, it can be seen that the addition of boric acid did had a beneficial effect at 40 pph, with a smoke color of white and medium smoke quantity. However this was not a large improvement from the RHA with no BA added. The 50 pph sample produced black smoke in high quantities which was worse than the 40 pph sample. Because the BA/RHA sample did not increase the fire resistance or decrease the smoke quantity substantially, it was rejected for further testing.

4.3.2.3 CG

For the 5% gypsum, the smoke was black, and had the highest amount of smoke development. However, as the % of gypsum increased, the color became white, and the amount of smoke released decreased. For resins with 30% gypsum or more, the smoke released was low, and for 50% there was no smoke released since the sample never ignited. From this data as well as the fire results above, it can be concluded that the optimal additive is gypsum at a 50% concentration. Because of this, the CG was selected for additional testing.

4.3.2.3 CLS

The CLS's smoke results were not good. All of the samples lower than 40% developed black smoke, and all of the samples below 30% developed high amounts of smoke. This did not improve from the controls, and in fact was worse than the 1% control's smoke results. However, the smoke results for 30% or greater CLS was low, and the smoke development was low; both of which are an improvement from the controls.

4.3.2.4 Conc

Since the 70 pph sample did not ignite, there was no smoke produced. However, after the sample was forced to ignite, the amount of smoke was low and the color was white. Therefore, between these results and the results from the fire tests, this sample has been selected for additional testing.

4.3.2.5 FG

The 10, 30, 40 and 50% FG samples all produced low quantities of smoke, and the 30, 40 and 50% FG samples had white smoke while the 10% sample had a combination of white and black smoke. This is a large improvement from the controls which produced black smoke and at least medium quantities. Also, when compared to the CG, the FG samples all performed better except the 20%,

which is considered a mistest. While the fire results were not as good as the fire results from the CG, they were comparable, and therefore due to the smoke and fire results, the FG was selected for further testing.

4.3.2.6 FLS

The smoke development for the FLS was an improvement from the control for all the systems, but was not as good as the gypsum. The color of the smoke for the 5% and 10% samples was a mixture of black and white, indicating that both the paper and the resins were ignited and one was creating black smoke while the other produced white smoke. However, without the removal of the paper backing it is hard to tell which was producing which. The smoke development was highest for the FLS at 50% at high, and lowest at 30% with a "low" concentration. Since 30% FLS also produced white smoke, it can be concluded from the smoke and fire data that FLS resin systems performs optimally at a 30% FLS. However, it is not the optimal system that was tested.

4.3.2.7 NC

The best sample for the NC was the sample with 50% NC added. This sample had a smoke color of white and a quantity of medium; however, when compared to the 1% MEKP, the medium quantity is not an improvement. Also, for the 30 and 40% NC samples, they both produced very high amounts of smoke, which is worse than the results for the controls. In addition, the smoke color for the 30% was a mixed black and white, and for the 40% was a black color. While the black and white color is an improvement from the controls, this is not a good result.

4.3.2.8 RHA

As far as smoke development results, the RHA was the worst in terms of color. In every situation it except for the 5% RHA, the samples produced black smoke. In addition, all of the samples except the 5% RHA produced a high amount of smoke, and the 5% RHA produced a medium amount of smoke. However, the black smoke may be related to the fact that the RHA is black and therefore the smoke is black as well. From this as well as the results from the fire test, it can be concluded that the RHA system is the most efficient at 5%. This may be due to the fact that as the percent of RHA added to the resin increased, the workability of the system decreased, and therefore the amount of air voids increased which caused the flames the ability to reach the paper backing at quickly and to continue to continue to burn for longer durations.

4.3.3 Char formation

One of the mechanisms which provides the potential to create fire resistance is the formation of a char layer. In Table 16, whether a char layer formed or not is reported. Except for with the RHA and BA/RHA, the samples which formed a char layer preformed the best. Although the RHA and BA/RHA samples formed char layers, they were very soft with an excessive amount of air voids which caused the char layer to not be effective at insulating the resin system because the heat is able to propagate through the air voids.

Table 16: Formation of Char Layer

Additive	% Additive	Char Layer (yes/no)	Additive	% Additive	Char Layer (yes/no)
Controls	1% MEKP	No	Conc	70 pph	Yes
	5% MEKP	No	Fine Gypsum	10%	Yes
ATH	30%	Yes - Limited		20%	Yes
	40%	Yes		30%	Yes
	50%	Yes		40%	Yes
BA/RHA	40 pph	Yes		50%	Yes
	50 pph	No	Fine Limestone	5%	No
Coarse Gypsum	5%	No		10%	No
	10%	No		20%	No
	20%	Yes		30%	No
	30%	Yes		40%	Yes
	40%	Yes		50%	Yes
	50%	Yes	NC	30%	Yes
Coarse Limestone	10%	No		40%	Yes
	20%	No		50%	No
	30%	No	Rice Hull Ash	5%	Yes
	40%	Yes		10%	Yes
	50%	Yes		20%	Yes
				30%	Yes
				40%	No

4.3.4 Workability Limit

The additives which were most effective at providing fire resistance were as follows: ATH, CG, Conc, and the FG. Therefore a workability limit test was performed on all of these additives except

for the CG. A workability limit was not performed on the CG because the optimal amount of CG was already determined to be a fully packed sample. Therefore, workability limits were found for ATH 202 (ATH1), ATH 802 (ATH2), and Conc in both the special resin and the standard resin and FG was tested with the special resin. FG was only tested for the special resin because the preliminary tests showed that the idea amount of additives to add to the resin system was 40% of the system. The results for each type of additive can be seen in Table 17 for the standard resins, and Table 18 for the special resins.

Table 17: Workability Results for Standard Resin

	Concr+St Resin		**ATH 1 + St Resin**	
PPH	**Workability**	**Comments**	**Workability**	**Comments**
20	10		n/a	
30	10		n/a	
40	8		8	
50	7		8	
60	5	Goopy	7	
70	4		6	
80	3		5	
90	2	not workable, gritty	4	
100	1	Clumps	4	honey like
110	n/a		3	Un-pourable, still spreadable
120	n/a		3	very un-pourable, still semi-spreadable
130	n/a		2	waxy texture

	ATH 2 + St Resin	
PPH	**Workability**	**Comments**
40	10	
50	7	
60	6	
70	6	
80	5	
130	2	honey like

Table 18: Workability Results for Special Resin

	Concr + Sp Resin		ATH 1 + Sp Resin	
PPH	**Workability**	**Comments**	**Workability**	**Comments**
20	10		n/a	
30	9		n/a	
40	7		8	
50	6		7	
60	5	Goopy	6	
70	4	Chunky	5	
80	1	Unworkable	4	Honey like
90	1		3	Un-pourable, still spreadable
100	0		1	very un-pourable, still semi-spreadable
110	n/a		n/a	
120	n/a		n/a	
130	n/a		n/a	
	ATH 2 + Sp Resin		**FG + Sp Resin**	
PPH	**Workability**	**Comments**	**Workability**	**Comments**
20	n/a		n/a	
30	n/a		10	
40	8		10	
50	8		7	
60	7		7	
70	6		6	
80	6		5	
90	5		4	
100	4	Honey like	2	Goopy
110	3	Un-pourable, still spreadable	n/a	
120	2	very un-pourable, still semi-spreadable	n/a	
130	1	unworkable	n/a	

The ideal workability was determined to be 4, which is a unit less comparison between different the workability of different additive amounts based on the resin's ability to be spread. This was because at this value, the resin/additive mixture was still runny enough to soak through the fiberglass, and

still easily spread so it could cover the whole sample. Therefore, the additive amount which created a workability of 4 was selected. For the Conc, the ideal amount of additives was found to be 70 pph for both the special and standard resins. For the ATH1, the ideal amount of additives was found to be 100 pph for the standard resin and 80 pph for the special resin. The ideal amount of additives for ATH 2 was determined to be 110 pph for the standard resin and 100 pph for the special resin. Finally, for the FG the ideal amount of additives was found to be 90 pph for the special resin. Therefore, these amounts were used for the flame test with the special resins.

4.3.4 Special Resin Flame Test

A control sample of the Sp1 as well as Sp1 with Conc, ATH1, ATH2, FG and CG were created and a propane torch was applied for 10 seconds. None of the samples generated smoke and none of them ignited, so the torch was reapplied for an additional minute, and then removed. Again, none of the samples ignited, however the all produced small amounts of white smoke. After the heat was removed, the conc had lost its structural integrity, and therefore was eliminated as a candidate for further testing. The CG maintained its structural integrity, however, while the torch was being applied, the CG began to pop at approximately 20 seconds. Therefore the CG was also eliminated. Lastly, the FG was eliminated because it produced more smoke than either of the ATH samples.

4.4 Panel Tests (Preliminary ASTM E 119)

4.4.1 Single Panel Tests

4.4.1.1 Introduction

In order to determine the heat flow through the gypsum-fiberglass system, 2'x2' panels were created using the following materials: regular resin control, regular resin + ATH1, regular resin + ATH2, and an Sp1 control, all with the pph of the additive added according to the workability limits as discussed above. The 2'x2' panels were then cut into 1'x1' panels for testing, providing 3 panels of each type to test, and an extra in case one panel was damaged. In order to create the system, a hand-layup method was used, where a layer of 3 oz chopped strand glass fibers was used in conjunction with a polyester resin. The FRP system was cast by first wetting the gypsum wall board with resin, then applying the fiberglass, and then adding more resin. Air bubbles were then smoothed out, and the system was allowed to cure until tacky. Once the system was tacky, the foam was applied to the top of the FRP. The hope was that in so doing, the melting of the polystyrene by the resin would be minimized. A diagram of the gypsum-fiber glass system can be seen in Figure 2.

Figure 2: Panel Setup

4.4.1.2 Procedure

In order to test the panels, they were raised above the ground 50”, in order to provide accurate readings from the laser camera. In addition, a type k thermocouple was inserted through the foam in order to measure the temperature at the top of fiberglass. A propane torch, which burns at 1850 ^{0}C, was then applied to the panels with the propane flame beginning at 24” away from the panel. The torch was then moved ½” closer to the panel every five minutes. This was continued for two hours. Data was recorded with a thermocouple (type k) at the top of the fiberglass, and with the laser camera at the bottom of the gypsum. The testing system can be seen in Figure 3.

Figure 3: Testing system

4.4.1.3 Results

After each experiment had been concluded, the system was deconstructed to visually analyze the results of the flame test. From this, the effects of the heat on the bottom of the gypsum, top of the gypsum, FRP and on the foam were compared. For the gypsum, the amount of gypsum burned was compared. For the FRP, the color of the resin and the burn pattern were compared. For the polystyrene, the amount of melting, and the melting characteristics were compared. In addition, the heat generated at two points was compared from one test to another: 1. At the bottom of the gypsum, 2. At the top of the fiberglass.

4.4.1.3.1 Gypsum

4.4.1.3.1.1 Bottom

On the bottom of the gypsum, the effects of the flame were constant regardless of the resin type or additives used. Throughout all the tests, the bottom of the gypsum reacted constantly with the following steps, which are shown in Figure 4 (A)-(C) below:

1. After ~1 hr, the gypsum started to blacken
2. After 1.5 hr, the gypsum started to glow
3. After 1.83 (1 hour, 50 minutes) the gypsum began to ball up around the propane torch.

(A) (B) (C)

Figure 4: Changes of the gypsum over two hour at (A) 1 hr, (B) 1.5 hrs, (C)1.83 hrs

4.4.1.3.1.2 Top

The reaction to the heat at the top of the gypsum was only able to be analyzed visually; however, it was always the same regardless of the matrix. The results for this were always a slightly charred spot directly above were the heat was applied to the bottom of the gypsum.

4.4.1.3.2 FRP

After the testing had concluded, the system was disassembled and the fiberglass was examined. The following are the results from each different type of matrix.

4.4.1.3.2.1 RR Control:

The FRP was charred black color. From inspection, it was observed that the FRP had caught on fire.

Figure 5: RR control FRP

4.4.1.3.2.2 RR+ATH1/ ATH2

As seen in Figure 6 (A), the RR+ATH1 was light brown color, indicating that it did heat up, but it did not char. Figure 6 (B) shows the results for the RR+ATH2. The results for the ATH1 and ATH2 are similar colors; however, the ATH1 is a constant brown color while the ATH2 has a lighter ring on the inside.

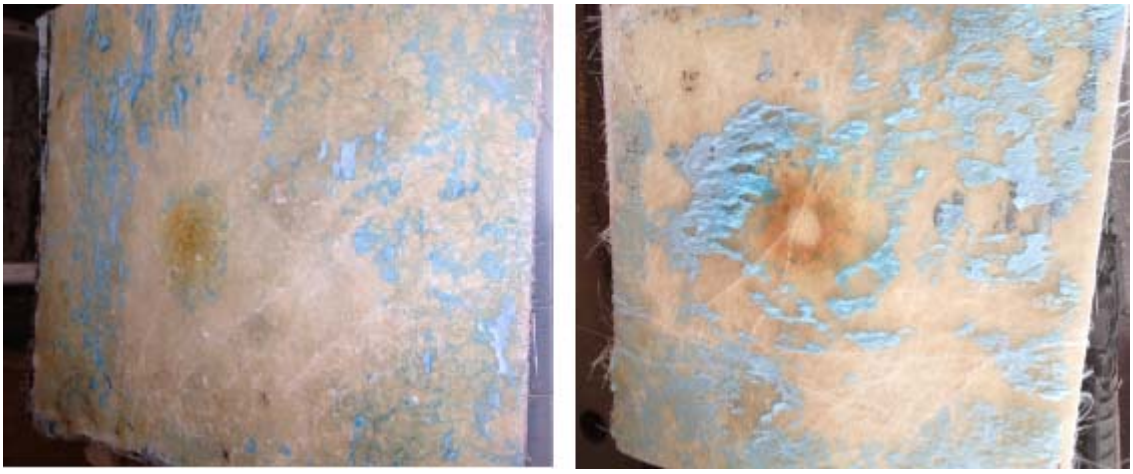

(A) (B)

Figure 6: (A): RR + ATH1 FRP (B): RR + ATH2 FRP

4.4.1.3.3 Foam

Although the heat flow through the gypsum and FRP was constant from system to system, as discussed below, the foams reacted differently. The best cases were the regular resin+ ATH1 and ATH2. Neither of these systems had large amount of melting or produced a high amount of fumes. These results can be seen in Figure 7.

(A) (B)

Figure 7: Foam melting for (A) RR+ATH1, (B) RR+ATH2

The RR control had the highest amount of melting, and even melted a softball sized hole in the foam which propagated though the thickness of the 2" foam. While the RR control had the highest amount of melting compared to the other systems, it did not have the highest amount of fumes produced. The time at which the foam began to melt was able to be determined via smell; however, the smell was not overwhelming. The results of the RR control's melting can be seen below in Figure 8.

Figure 8: Foam melting for RR control

While the systems with regular resin all melted the foam in a circular fashion, the FRR did not. The foam melted more in the shape of vents, as can be seen in Figure 9. While it does not look as if the foam in the FRR system melted much, it did melt through the foam. However, this was not the 2" of foam that were cast. While 2" of foam was originally applied to the top of the FRP, since the FRR

requires more time to cure, it was able to melt the foam during curing. Therefore, when the test was started, only approximately ½" of foam covered the FRP and gypsum. However, during the test, it was noted that the FRP was smoking through the foam, and that that smoke was pungent.

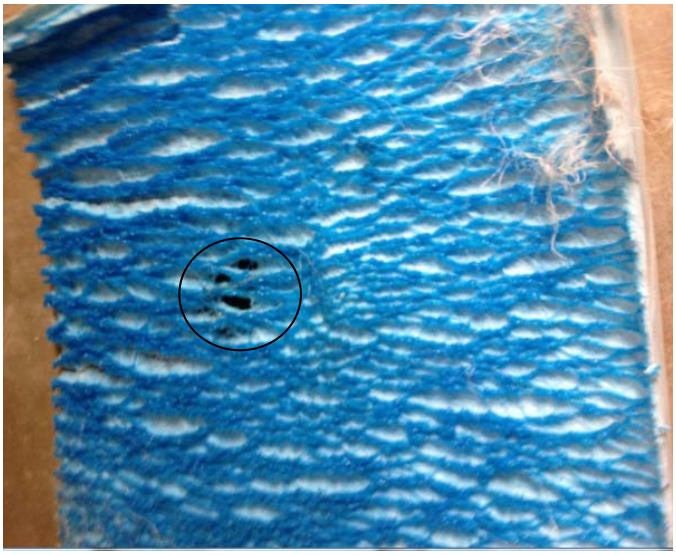

Figure 9: Foam melting for FRR control

4.4.1.3.4 Comments

Because of the difference between the melt patterns between the RR control and RR+ATH1 and ATH2, it indicates that the FRP also serves to disperse and deflect heat flow in the system.

4.4.1.3.5 Heat Flow

The heat flow was measured on the bottom of the gypsum with a laser camera and on the top of the FRP with a type k thermocouple. From the data, graphs were developed of the heat flow through each system. It was found that the heat flow was approximately equal for each system. The exception to this was for the RR control. Errors occurred while measuring the heat flow because of the difficulty of perfectly lining up the thermocouple and the propane torch. However, after it was noticed that this was affecting the data, extreme care to line them up was taken. Graphs of the heat flow through the FRR control can be seen in Figure 10. The line marked as max is the temperature recorded at the bottom of the gypsum and the line marked TC is the temperatures recorded at the top of the FRP. According to the graphs, the foam began to melt after 6398 seconds (107 minutes), which has been marked with the vertical line. For all of these tests, the temperature where the flame was applied corresponds to the primary (left hand) y-axis, and the temperature at the top of the FRP is along the secondary (right hand) y-axis.

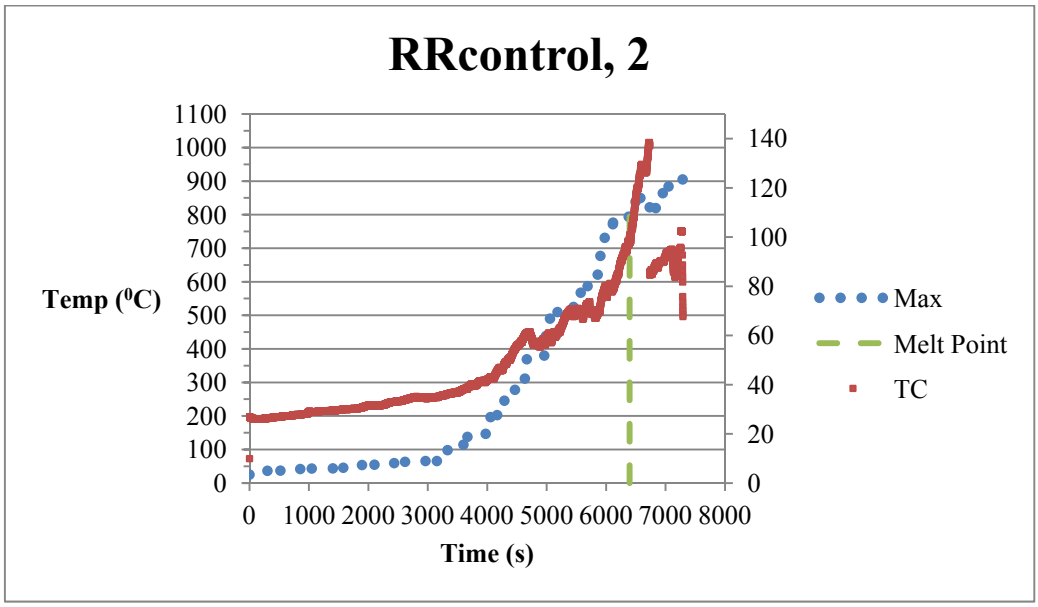

Figure 10: Time vs. Temperature curve for RR control

The heat flow for the rest of the systems remained fairly constant, and can be seen below in Figure 11. The average time to melt was 7055 seconds (118 minutes), which is two minutes below the two hours.

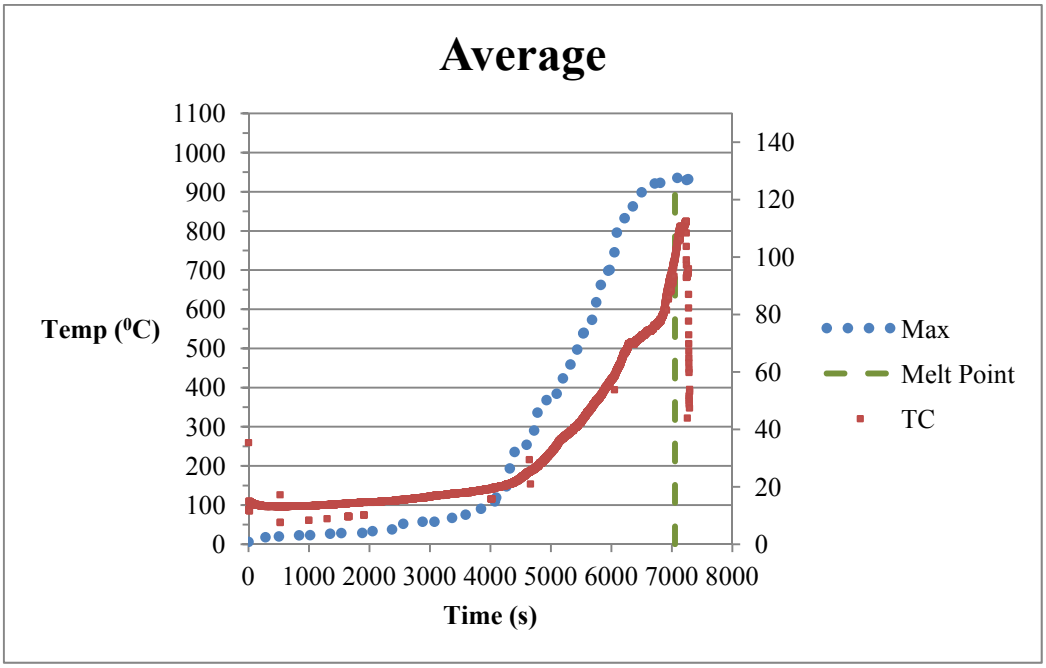

Figure 11: Time vs. Temperature curve between ATH1, ATH2 and FRR Control

While the time to melt was constant throughout the samples, the amount of melting that occurred was not constant. This may be due to the heat distortion temperatures, which is the temperature at

which the FRP begins to lose its structural integrity. The heat distortion temperatures are 106 ^{0}C and 96 ^{0}C for the regular resin and the fire resistant resin, respectively.

4.4.2 Double Panel Tests

4.4.2.1 Introduction

After it was discovered that the heat distortion temperature was met when using a single layer of gypsum, three double panel tests were performed in order to determine whether this was a satisfactory thickness to keep prevent either the foam from melting or the FRP from reaching its heat deflection temperature. This was conducted by gluing two 5/8" thick layers of gypsum together with isophthalic resin. The resin was then allowed to cure, and the same procedure was performed as with the single-panel tests, but with no FRP or foam included in the test, simply the gypsum. Therefore, the thermocouple was able to be attached directly to the gypsum. This reduced some of the error as it was hard to with the foam if the thermocouple was actually in contact with the top of the FRP.

4.4.2.2 Results

After each experiment had been concluded, the top and the bottom of the gypsum was analyzed in order to visually judge the effects the heat had. As before, the amount of gypsum burned was compared. Also, the heat was compared at the top and bottom of the gypsum panels.

4.4.2.2.1 Bottom

The results for the bottom of the gypsum were consistent with the results from the single panel test and as shown Figure 4 (A)-(C) above.

4.4.2.2.2 Top

The top of the gypsum was unmarked at the end of the test. There was no sign of charring as can be seen below in Figure 12, and the gypsum was slightly warm to the touch.

Figure 12: Top of Gypsum after Double Panel Test

4.4.2.3 Heat Flow

The heat flow through the system was measured as with the single panel test with a type k thermocouple on the top of the gypsum, and with a laser thermometer on the bottom of the gypsum. From this, graphs were developed for each panel tested as well as the average temperature across all three systems. In addition, the maximum temperature at the top of the gypsum was recorded and the total amount of time for each test was recorded. The graphs were then compared for accuracy, and tests were repeated as needed. The average temperature through the systems can be seen below in Figure 13 where the "max" data series is the bottom of the gypsum where the heat was applied and "TC" is the top of the gypsum where the thermocouple was positioned. The max data series corresponds to the primary, left-handed y-axis, while the TC data series corresponds to the right-hand secondary y-axis.

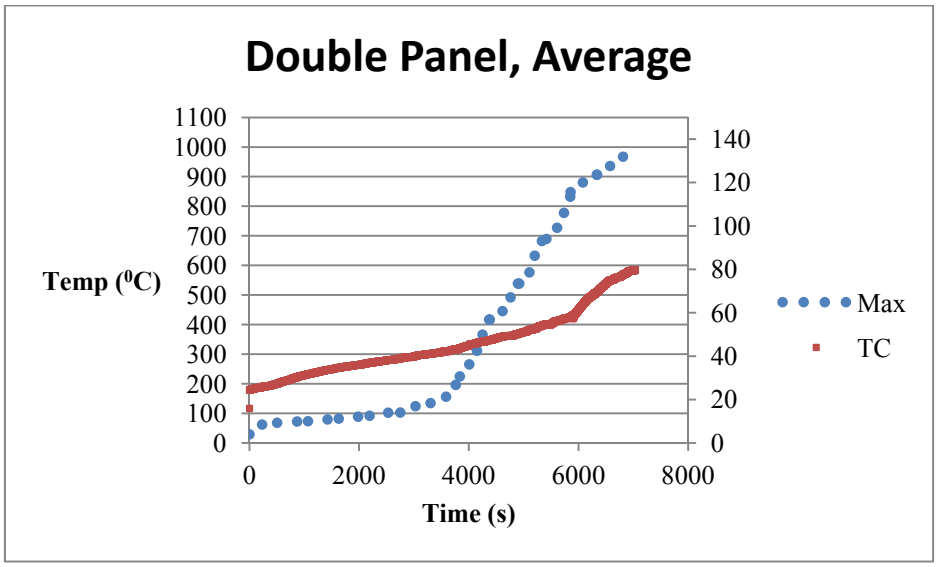

Figure 13: Average Double Panel Test

From this graph, it can be seen that the temperature at the top of the gypsum remains below the heat distortion temperature. The exact numbers for this are summarized below in Table 19 below. While the temperatures at the bottom of the panel were around 990 ^{0}C, the temperature at the top of the panels remained around 83^{0}C, which is 13 ^{0}C and 23 ^{0}C below the heat distortion temperatures for the regular resin and the fire resistant resin, respectively. Therefore, two 5/8" thick gypsum panels are sufficient insulation to prevent the foam from melting.

Table 19: Double Panel Test Information

Max Time (min)			Max Temp (^{o}C) Bottom				Max Temp (^{o}C) Top			
P 1	P 2	P 3	P 1	P 2	P 3	Ave	P 1	P 2	P 3	Ave
122	126	128	979.8	985.3	996.4	990.9	85.1	78.8	83.9	82.6

4.5 Flame Spread Tests (Preliminary ASTM E 84)

4.5.1 Introduction

A flame spread test was required to better determine the best resin/FRP combination by determining how far the flame would spread for different resins and additive amounts. In order to accomplish this, FRP was cast onto cement wallboard. The systems tested were as follows (2) RR controls, (2) RR + 50% ATH1, (2) FRR control, and (2) RR + 50% ATH1. The FRR systems were both mixed with 2% cobalt to accelerate the cure time. After the samples had cured, a propane torch was applied to them for ten minutes or until the flame spread stopped, as shown below in Figure 14. Rulers were

placed to the side of the specimen to show on camera the extent of the flame spread, as well as to confirm that the heat was applied in the center of the sample.

Figure 14: Flame Spread Test Setup

The distance that the flame had spread was then measured. In addition to the flame spread, the amount of smoke generation was quantified from very low to high, the smoke color was recorded, and whether an odor was produced was recorded as well as the intensity of the odor. It should be noted that tests were performed in well ventilated areas. The results for these tests can be seen below in Table 20. From this table it can be seen that RR control and the FRR control both preformed similarly, both with a maximum flame spread of 8 inches and an average flame spread of 7.5 inches. However, the smoke generation for the FRR resin was significantly greater and had a higher odor. The best resin for reducing flame spread was the RR+ATH1, with a maximum flame spread of 5 inches and an average flame spread of 4.75 inches. In addition, RR+ATH1 generated a minimal amount of odorless white smoke. Therefore, for the RR+ATH1 can be concluded to be the optimal resin for the flame spread test.

Table 20: Flame spread results

Sample	Flame Spread (in)	Smoke Generation	Smoke Color	Odor?
RR control (1)	8	Medium	Black	Yes - High
RR control (2)	7.5	Medium	Black	Yes - High
RR control (Ave)	7.75	Medium	--	--
RR+ATH1 (1)	4.5	Very Low	White	No
RR+ATH1 (2)	5	Very Low	White	No
RR+ATH1 (Ave)	4.75	Very Low	--	--
FRR control (1)	8	High	Black	Yes - Medium
FRR control (2)	7	High	Black	Yes - Medium
FRR control (Ave)	7.5	High		--
FRR+ATH (1)	6	Medium	Black	Yes - Low
FRR +ATH (2)	6.5	Medium	Black	Yes - Low
FRR+ATH (Ave)	6.25	Medium	--	--

4.6 Mathematical Model

A heat flow model of the system was developed to confirm the findings from the double panel test. First a 1-D steady state model was used to provide an upper bound for the values. Then an unsteady state model was created.

4.6.1 Steady State Model

For the steady state system, the following assumptions were made:

1. The system is semi-infinite
2. The heat flux (q) through the system is constant.

First, the heat flux across the air was determined given that the temperature of propane is 1850^0C, and that when the propane torch was 5/8" away from the FRP, the temperature of the FRP was equal to 914^0C. In order to find the heat flux, Eq. 4.1 was used as shown below.

$$q = \frac{Tp - T1}{\Sigma R} \qquad \text{Eq. 4.1}$$

Where T_p is the temperature of the propane (K) which is 2123K, T_1 is the temperature of the bottom of the gypsum (K) which is 1187K, and R is the sum of the resistances through the system as found from Eq. 4.2 below.

$$R = \frac{L}{K * A} \qquad \text{Eq. 4.2}$$

Where L is the thickness of the layer (m), K is the conductivity of the material (W/m*K) and A is a unit (m^2).

Table 21: Steady State Heat Flow Values

	K (W/m*K)	L (in)	R (K/W)
Air	0.068	5/8	0.235
Gypsum	0.258	1 1/4	0.123
Composite	0.588	1/8	0.005
Foam	0.033	2	1.539

Using the values for air from Table 21 as well as Eq. 4.1 and Eq. 4.2, the heat flux was found to be 3982.437 W per unit area. From this, the temperatures at each layer in the system were determined using Eq. 4.3 as defined below.

$$T_i - T_{i+1} = q * R \qquad \text{Eq. 4.3}$$

Where T_i is the temperature at the bottom of the layer (K), T_{i+1} is the temperature at the top of the layer (K), q is the heat flow in the system as determined above in W, and R is the resistance for each layer as determined from Eq. 4.2 and shown in Table 21 (K/W). By using this process, the temperature at each layer in the system was determined and is displayed in Table 22.

Table 22: Steady State Temperatures

	Temperature (^{0}C)	Location
Tp	1850	Propane
T1	914	Gypsum / Air Layer
T2	423.9	Gypsum / FRP Layer
T3	402.4	FRP / Foam Layer
T4	25	Top of Foam

Since this is for steady state conduction, this provides the upper bounds for the values. However, a transient, or unsteady state solution, is needed to confirm the data from the experiment and to satisfy the building code.

4.6.2 Unsteady State Model

After the steady state model was created, an unsteady state model was created. The unsteady state solution calculated more accurate results, instead of just an upper bound as the steady state model

did. The temperatures calculated from the steady-state model were significantly greater than the temperatures found from testing, and provided an upper bound, therefore it was concluded that the temperature in the system had not had sufficient time to develop to a steady state solution. In order to create an unsteady state solution, the system was modeled in Comsol. Comsol is a finite element system for heat flow.

4.6.2.1 Setup

The model was constructed using the same material thicknesses as for the unsteady state model, as can be seen in Table 21 under the "L" column. The system may be seen below in Figure 15. The flame from the propane torch was approximated to be ¼" in diameter, and so the heat was applied to the bottom of the system in a ¼" strip. The applied heat was determined from the data, and was the average heat after the heat on the bottom of the gypsum began to increase or 839.82K (566.82 ^{0}C). The Comsol model was solved using a time step function of 7200 seconds (2 hrs). In addition, a surface convection (h) was applied to the bottom of the gypsum. Since the application of the propane torch causes forced convection, a reasonable estimate for the convection is 25-250 W/(m^2•K) (Welty, Wicks, Wilson, & Rorrer, 2008), therefore a surface of 100 W/(m^2•K) was selected.

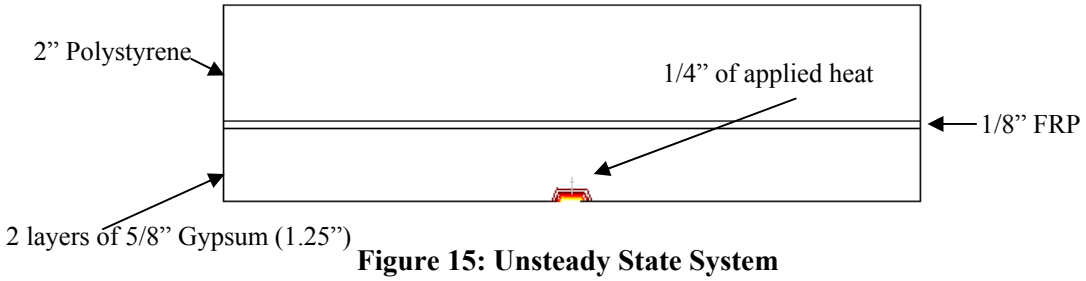

Figure 15: Unsteady State System

The thermal properties for the materials are summarized in Table 23. These values were determined from (Chen & Davalos, 2010) for the density of FRP, (Gibson, 2007) for the heat capacity and heat thermal conductivity of the fibers and matrix. The properties for polystyrene were found from the MSDS from DOW for polystyrene foam.

Table 23: Unsteady State Thermal Properties

	Gypsum	FRP	Polystyrene
k (w/m*K)	0.258	0.588	0.033
rho (kg/m^3)	2787	1522	1300
Cp (J/kg*K)	1090	18.217	24.829

Both a refined mesh and a coarse mesh were used to produce a solution. However, when the solutions were compared, the difference between solutions was within a degree, therefore in order to save time and space, the coarse mesh was used for analysis. These two meshes may be seen in Figure 16 and Figure 17.

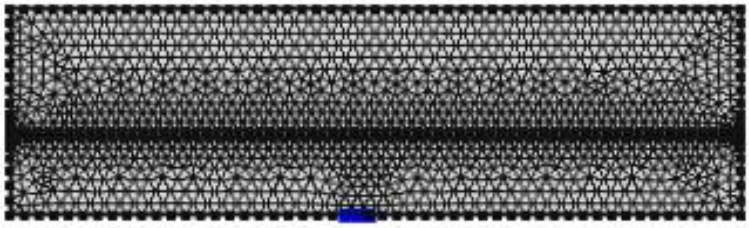

Figure 16: Fine Mesh

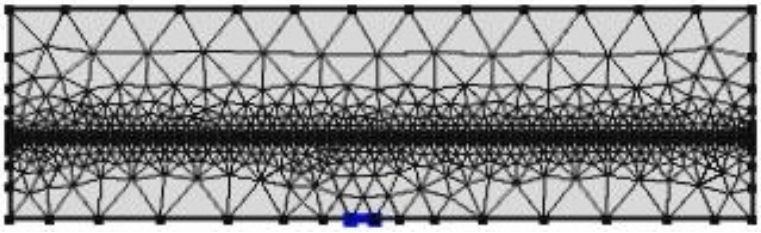

Figure 17: Course Mesh

For the course mesh, Comsol reached a solution in 14 seconds. The convergence study can be seen below in Figure 18.

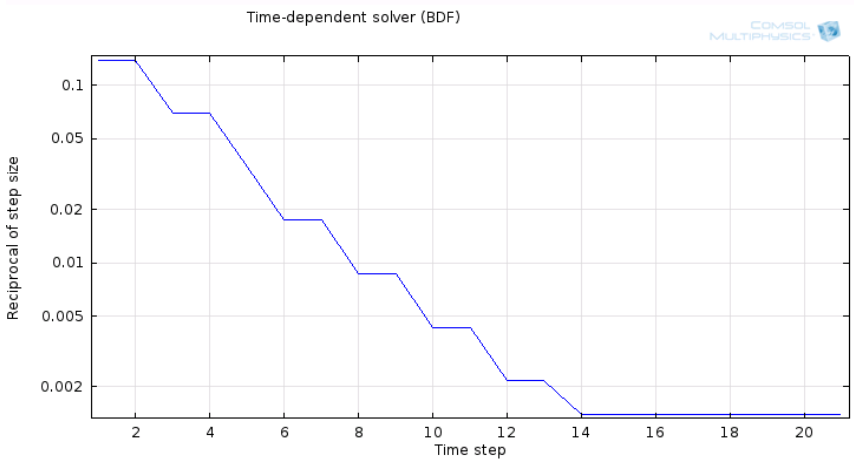

Figure 18: Comsol Convergence Study

4.6.2.2 Results

From the results of this model, the influence the heat had on the model was generated in a three dimensional picture which can be seen in Figure 19, which is the influence at 7200 seconds, or the end time. In order to create this model, a cut was made through the center of the model, so that the influence was able to seen with better precision. From this, it can be seen that the semi-infinite model is an appropriate model, as the heat dissipates to room temperature before the edge of the twelve inch plate regardless of the time.

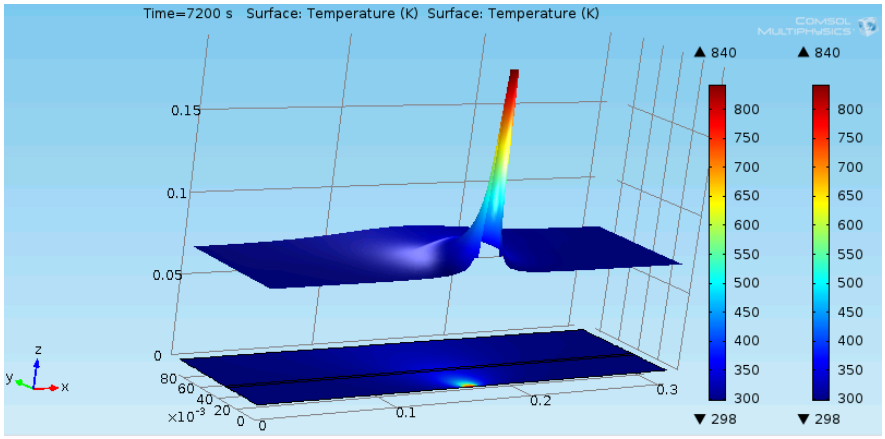

Figure 19: Influence of Applied Heat

One of the assumptions of the steady-state model is that the heat flux (q) throughout the system is constant. In the unsteady state solution, the heat flux is not constant; therefore q varies through the system as a function of temperature and position in the x and y-directions. A graph of the different gradients of heat flux was produced and can be seen in Figure 20. Note the scale on Figure 20 in both the x and y-directions where the x and y coordinates align with position of the system in the respective direction in inches.

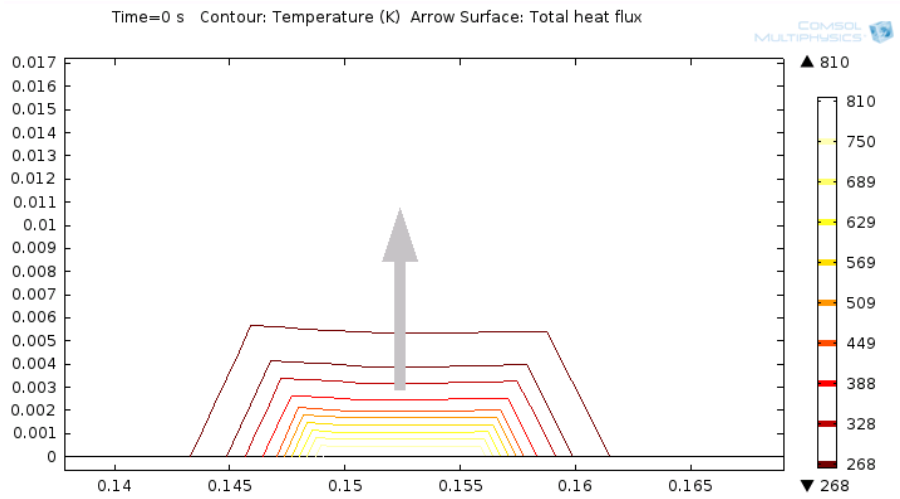

Figure 20: Heat Flux through System

Lastly, the change in temperature was plotted versus the position in the y-direction. This graph may be seen below in Figure 21. From this graph, it can be seen that the temperature at the top of the foam is 50^0C, which is an asymptote for the temperature. Figure 22, which limits the x-axis (y-position) to be between 1" and 1.5", was developed to determine the temperature between the gypsum and the FRP. The y-axis has been limited between 80^0C and 100^0C. From this, it can be seen that at 1.25", or at the boundary between the gypsum and FRP, the temperature from the Comsol model is about 89.5^0C. When compared to the temperatures for the heat from the experimental data, the average of which is 82.6^0C, the results from the Comsol model are 6.9^0C higher than from experiment. However, this may be attributed to the fact that the applied heat of 839.82K was the average temperature over the second hour, but was applied for the entire two hours. Another reason this may be is that the convection of 100 W/(m^2•K) may have been an underestimate of the convection in the system. However, it may be concluded that this is a good model of the system. Therefore, it can be found that at the top of the FRP, the temperature is approximately 88^0C. These temperatures are also well below the heat distortion temperature of the resin, and therefore it may be concluded that two 5/8" gypsum panels are sufficient to prevent the foam from losing its structural integrity.

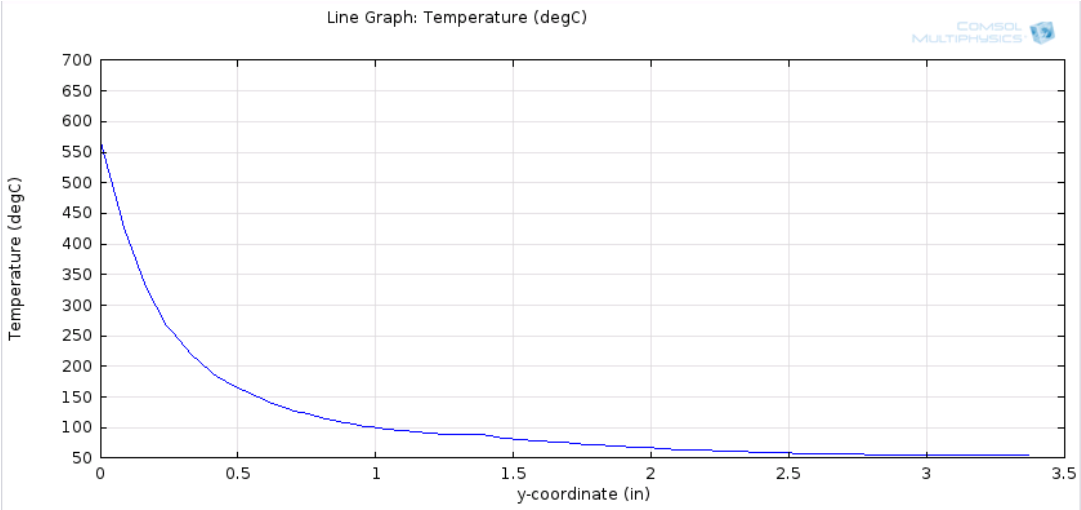

Figure 21: Temperature with Respect to Position

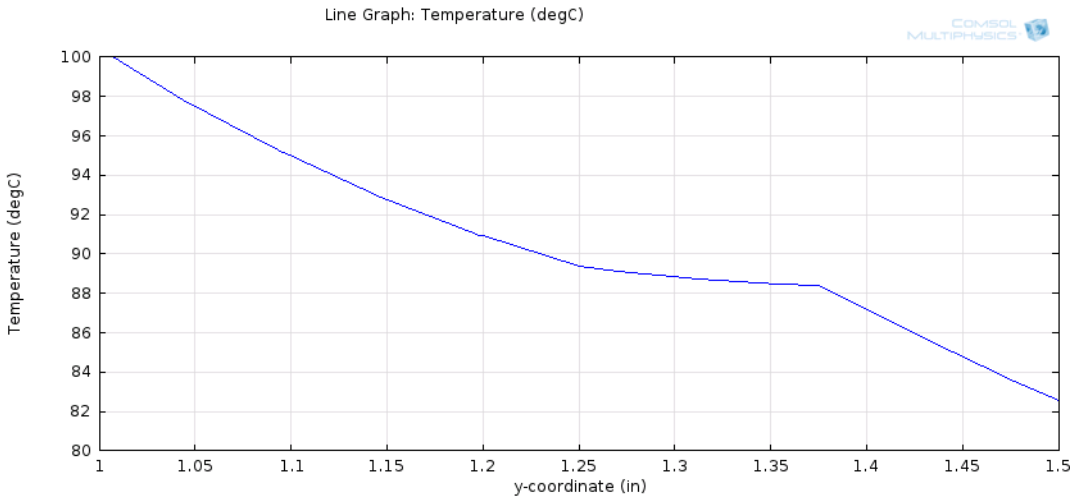

Figure 22: Temperature with Respect to Position, Zoomed in

4.7 Conclusion

From the tests conducted in this chapter, the following may be concluded

1. ATH is the ideal additive for isophthalic resin based on its fire-resistive properties
2. The flame spread for is best for the regular resin with ATH added
3. Two 5/8” gypsum wallboard panels sufficiently insulate the foam from losing its structural integrity
4. The system does not reach steady state during the panel tests, and therefore an unsteady state solution using Comsol, which is a finite element model that determines the heat flow and temperatures in the system, is the best method for producing a model of the system.

5. The Comsol model confirms that the data from experiment are accurate

From this, it may be concluded that, the standards set forth by the IBC for fire resistance in plastics may be obtained by adding ATH to isophthalic resin. However, additional research must be done to investigate the effects varying quantities of ATH has on the mechanical properties of the laminate. This study is addressed in Chapter 5.

Chapter 5: Mechanical Tests

5.1 Introduction

In order to determine the effects of ATH on mechanical properties, samples were tested for compression, flexure, shear and tension according to ASTM D695, D790, C1292 and D638 respectively. Tests were performed using an MTS machine with a maximum loading capacity of 22000 lbs. GFRP panels with various quantities of additives were first cast using vacuum bagging method, then cut to ASTM standard sizes and then tested. Before testing, the tension specimens were filed down to a thickness of 0.25" so that they could fit into the tension grips.

5.2 Samples

Samples were cast using vacuum bagging methods. First, a layer of visqueen was placed down, then a breather cloth, then peel ply. Next, the one layer 3 oz layer of chopped strand fiber was laid down, and the appropriate amount of resin, by weight, was added. After the resin had been applied, the system was pressed down to eliminate air from the system. The process with the resin and the fiber was repeated until the appropriate number of layers had been reached. After the FRP was cast, peel ply was placed on top, then another layer of breather cloth, and then the visqueen was folded on top, and the bag was sealed. Before the vacuum bag was opened and the FRP was removed, the FRP was allowed to cure for a minimum of twenty-four hours. Examples of this process can be seen in Figure 23 (A) and (B).

(A) (B)

Figure 23: Vacuum Bagging Process A) FRP sealing bag B) After sealing bag

In order to create the FRP samples, three two foot by two foot samples were cast with additive quantities of 0%, 25%, and 50% by weight of the total amount of resin. This means that if 50% was used, 50% of the system was resin, and 50% of it was ATH. Using a volumetric fraction of the fiber

(v_f) of 0.1877 (Chen & Davalos, 2010) for each 3 oz layer of fiberglass, the required weight of the resin was determined to be 26.37 oz per layer. Since the desired thickness of each panel was 0.25", the required number of plies was calculated to be four.

The resin additive mixture was created by weighing out the amount of additive per layer that was to be used. Next, resin was measured into paper bowls and premeasured ATH was added. The ATH was then carefully mixed into the resin in order to avoid creating air bubbles. Next, 5% MEKP hardener was added by weight of the total amount of resin. This was then also carefully mixed. Then the resin and additive was poured onto the FRP and smoothed evenly over the entire surface. After the resin had been spread over the FRP, a roller was used to eliminate air pockets between layers of fiberglass. This process was repeated for each layer of FRP. The goal was to achieve a ¼" thickness; however, the 50% ATH system was thicker. This is because at 50% ATH, the resin is too thick to properly soak the fibers.

After the composite had cured for a minimum of twenty-four hours, it was removed from the vacuum bag and placed under a fume hood until it was cut into the testing specimens. From each two foot by two foot panel, six specimens for each test were cut according to their ASTM standard measurements. Compression was cut to be 0.5" x 3.2", as can be seen below in Figure 24. The flexural specimens were cut to be 2" x 15", as can be seen in Figure 25. The sample for shear was a 0.75" x 3.0" tab, with 45^0 notches cut from the middle of the 3.0" span as shown in Figure 26. The tension test was a 10.0" x 1.0" tab with 3" tabs at each end for the tension grips to hold. After the 3" tabs, the tension grips narrowed to only be 0.5" wide as shown in Figure 27.

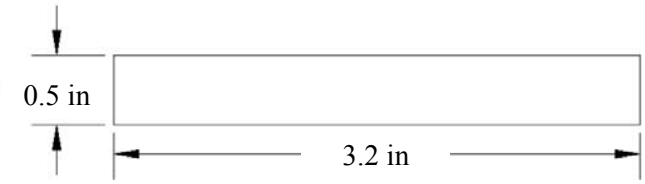

Figure 24: Compression Dimensions

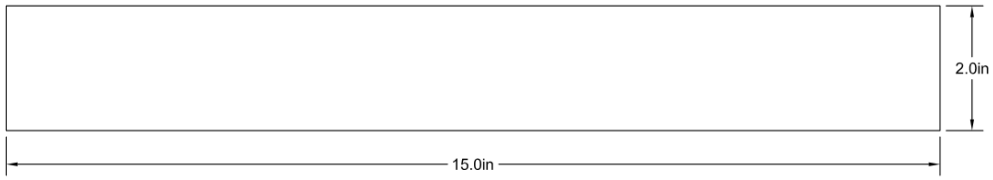

Figure 25: Flexure Dimensions

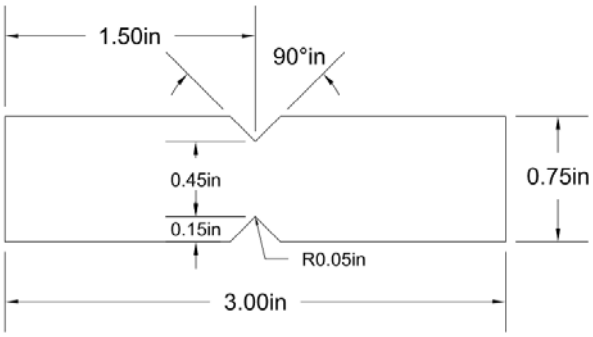

Figure 26: Shear Dimensions

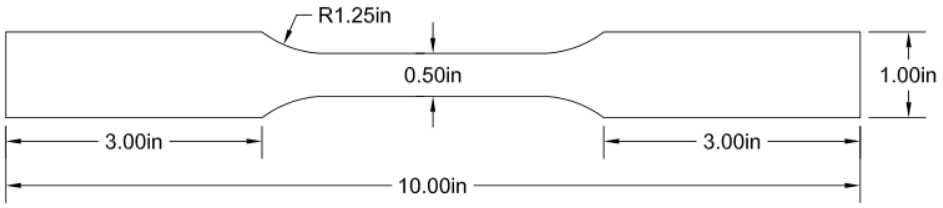

Figure 27: Tension Dimensions

5.3 Testing - Methods

5.3.1 Strain Gage Placement

Strain gages were placed on the compression, flexure and tension samples in order to measure the strains. No strain gages were used for the shear specimens, however, accuracy was checked by comparing the results to previous studies. For each test, strain gages were attached to four of the five samples for each of the different additive quantities (0%, 25%, 50%). Wires were then soldered to each of the strain gages, and data was recorded a data acquisition system. After the wires were attached, they were covered with electrical tape to prevent damage until testing. The tape was removed before testing.

5.3.1.1 Compression

For compression, one strain gage was placed at the center of the compression specimen. On the Boeing Modified Fixture, there is a space between where the fixture is and where the strain gage is placed to ensure that the strain gage is not damaged. This system can be seen below in Figure 28.

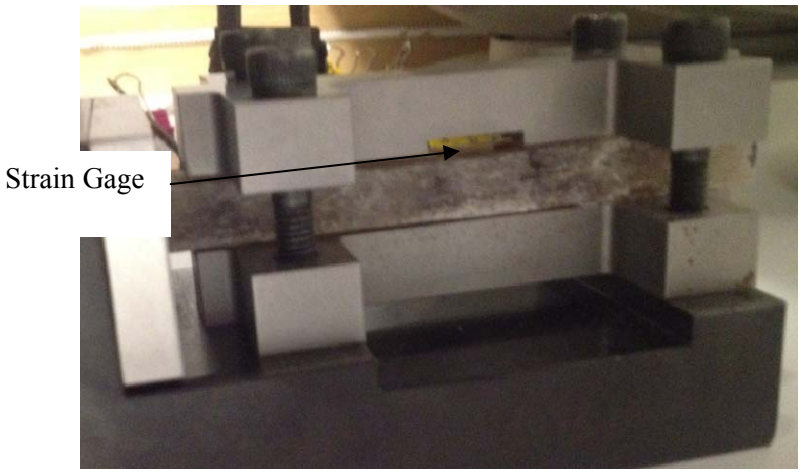

Figure 28: Placement of Compression Strain Gage, Example of Compression Fixture

5.3.1.2 Flexure

For flexure, two strain gages were attached to the top and bottom of each of the required samples at the center of the sample. Therefore, they were attached 7.5” from the end and 1.0” from the midspan as can be seen in Figure 29.

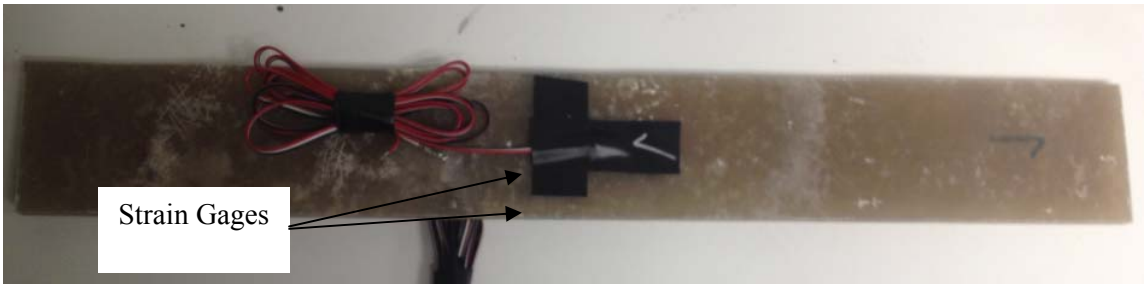

Figure 29: Placement of Flexure Strain Gage

5.3.1.3 Tension

For the tension tests, a strain gage was placed at the middle of each of the required specimen, therefore the center of the strain gage was placed 5” from the end of the tension specimen. This system can be seen below in Figure 30.

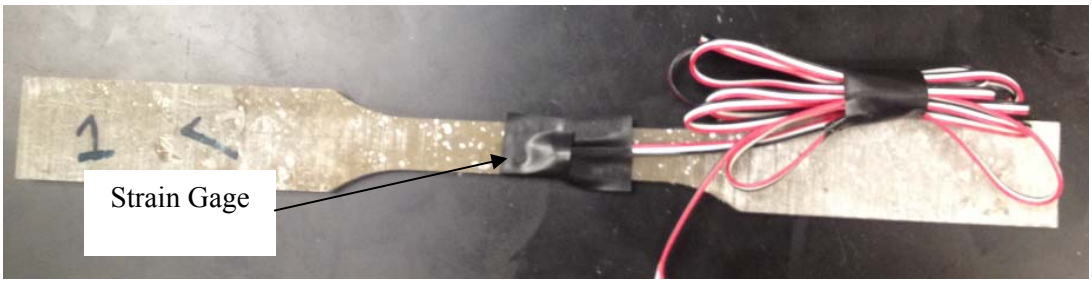

Figure 30: Placement of Tension Strain Gage

5.3.2 Loading Rates

For each test, loading rates were used as specified by their respective ASTM standards. These standards can be seen below in Table 24. These values were entered into the MTS machine, which was set up to be deflection controlled.

Table 24: Loading Rates

ASTM	Test	Loading Rate
Modified D 695	Compression	0.05"/min
D790	Flexure	0.05"/min
D638	Tension	0.2"/min
C1292	Shear	0.33"/min

5.3.3 Methods

5.3.3.1 Compression (ASTM D 695)

For the compression testing, the samples were placed in the fixture as shown in Figure 28. The bolts were then hand tightened to the point that there was a limited amount of resistance. This was done because if the bolts were lose the samples could buckle, but if they were too tight then the fixture and the sample could form a steel-GFRP composite. The buckling case would provide data resulting in strength that was less than the actual strength of the composite, while the composite cause would create a strengthened system, and therefore the values for the strength would be greater than the actual strength of the FRP.

5.3.3.2 Flexure (ASTM D 790)

For flexure, a three point bending test was preformed. For the test, a fixture was used with a span of 11 inches; therefore the sample extended past the fixture a total of 2 inches on each end. The load

was applied at the center of the sample, or 7.5” from each end of the sample, and 5.5” from each support. This setup can be seen below in Figure 31.

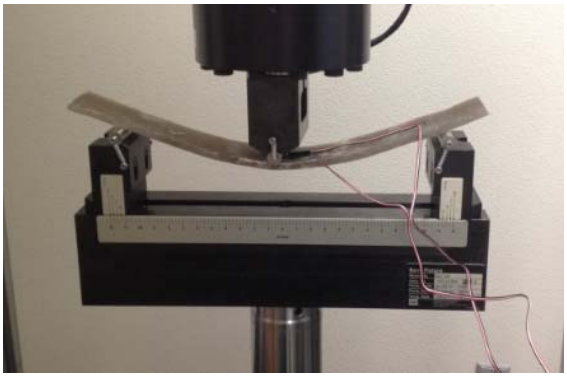

Figure 31: Example of Flexure Fixture

5.3.3.3 Shear (ASTM C 1292)

Each shear specimen was inserted into the fixture as can be seen in Figure 32. Care was taken to align the sides of V-notch with the edge of the supports. In addition, the specimen was aligned with the front of the testing fixture for consistency.

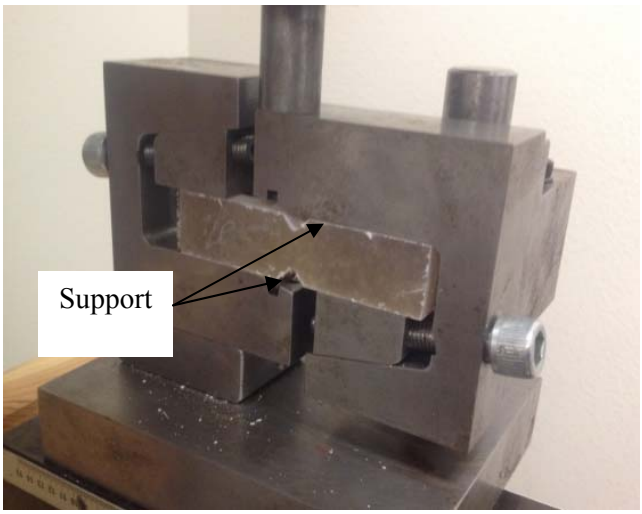

Figure 32: Example of Shear Fixture

5.3.3.4 Tension (ASTM D 638)

For the tension tests, Syntech grips were used. The grips were able to clamp samples that were up to 0.25 inches thick, therefore the samples were filed to a thickness of 0.23 inches in order to ensure that grips could tighten around them. The whole system was reduced in size, as to prevent failure from occurring at the grips; where the thickness, and therefore the strength, would be the smallest.

For testing, the grips were hand tightened around the samples until a force of 50 lbs was applied, and then the test was run. The system for the tension testing may be seen below in Figure 33.

Figure 33: Example of Shear Fixture, Failed Tension Sample

5.4 Results

The following summarizes the results from each test. Five specimens from each resin type were tested for each test. Four of these specimens had strain gages attached to them. After the data had been collected, the maximum stress and maximum deflection for the control samples were compared to previous studies on FRP to ensure accuracy (Chen & Davalos, 2010). Also, after each different resin type was tested, the force displacement curves for each specimen were developed and compared to each other. If an outlier existed, a new specimen would be cut and tested.

5.4.1 Compression Test (ASTM D 695)

5.4.1.1 Load, Deflection, and Stress

For the compression tests, a force displacement curve was developed from the MTS machine, and stress strain curves were developed both from the MTS machine and from the data acquisition system (DAS) and then compared to each other for validation. This comparison can be seen for the control in Figure 35, for 25% ATH in Figure 36, and for the 50% ATH in Figure 37. In addition, the

results from the MTS machine for the control resin were compared to previous studies to ensure validity, this can be seen below in Table 25. However, the strain gages stopped working at around 0.004 in/in due to debonding of the strain gages; and therefore, the maximum strain were not able to be obtained from this data. Because the strain gages failed while the material was still non-linear, the modulus of elasticity was unable to be calculated from the DAS. The force-displacement curve as seen in Figure 34 shows the strength of the composites given their areas, however, since the 50% ATH samples were 0.109 inches thicker on average thicker than the control and the 25% ATH samples are on average 0.006 inches thicker than the control, this must be taken into account for. Therefore, the stress-strain curve from the MTS machine as seen in Figure 38, which takes into account the area differences, is a better representative of the actual strength of the composites. Also, from this graph, the modulus of elasticity for each additive amount was calculated using a linear trend line. In order to add the trend line, first the non-linear sections were removed, and then a best fit line was created. The equations for the best fit line may be seen on the graphs, where the slope is the modulus of elasticity. The modulus of elasticity may also be seen in Table 25, and a comparison between the control, 25% ATH, 50% ATH, and the modulus from research may be seen in Figure 39. The difference between the values from the previous research and from this experiment is due from using different testing methods, but they are similar.

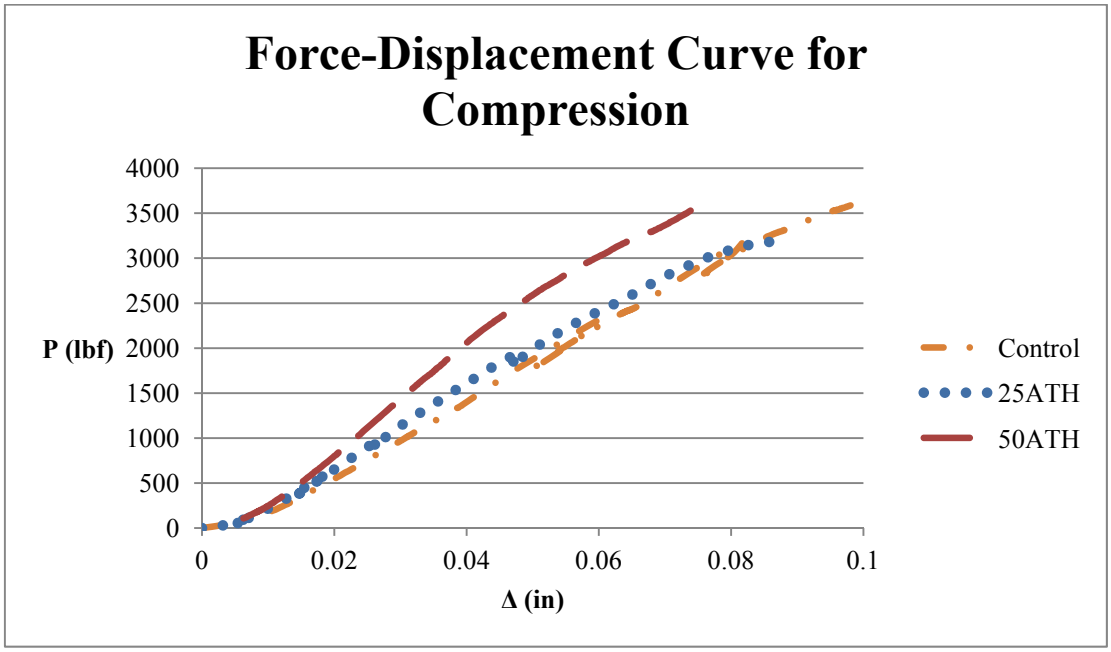

Figure 34: Force-Displacement Curves for Compression

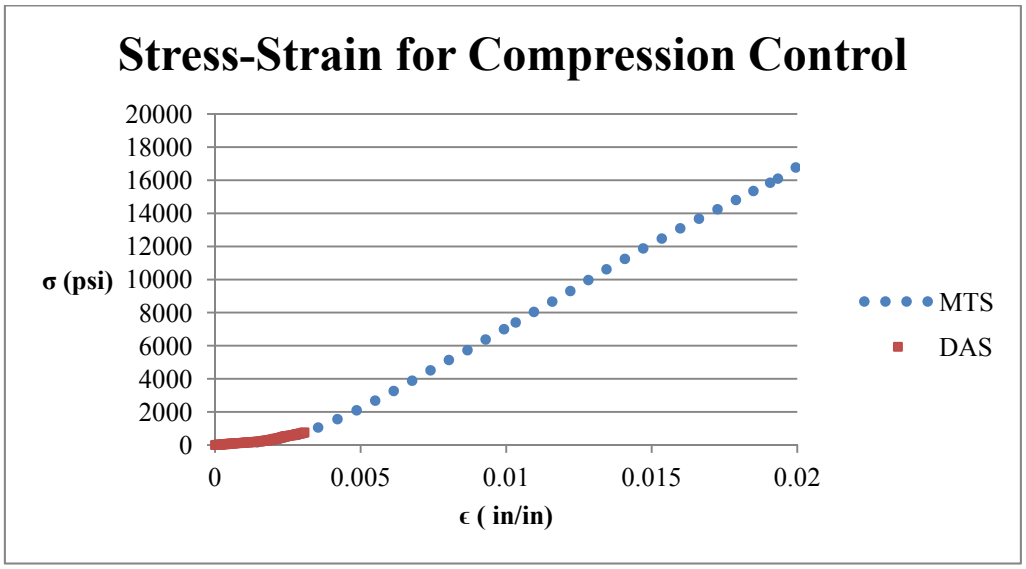

Figure 35: Comparison of Stress-Strain Curves of MTS and DAS for Control

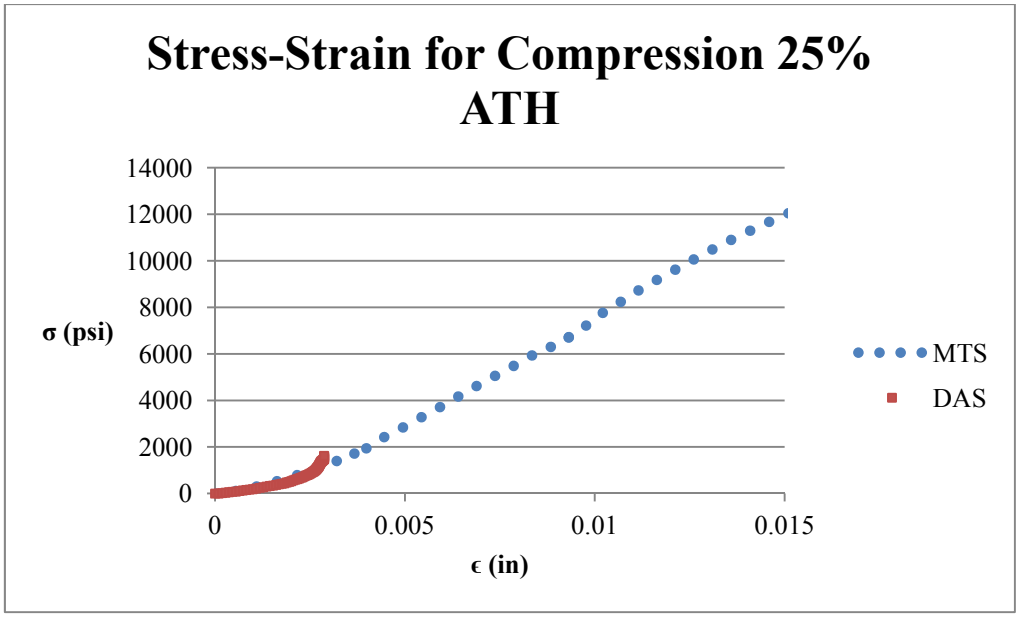

Figure 36: Comparison of Stress-Strain Curves of MTS and DAS for 25% ATH

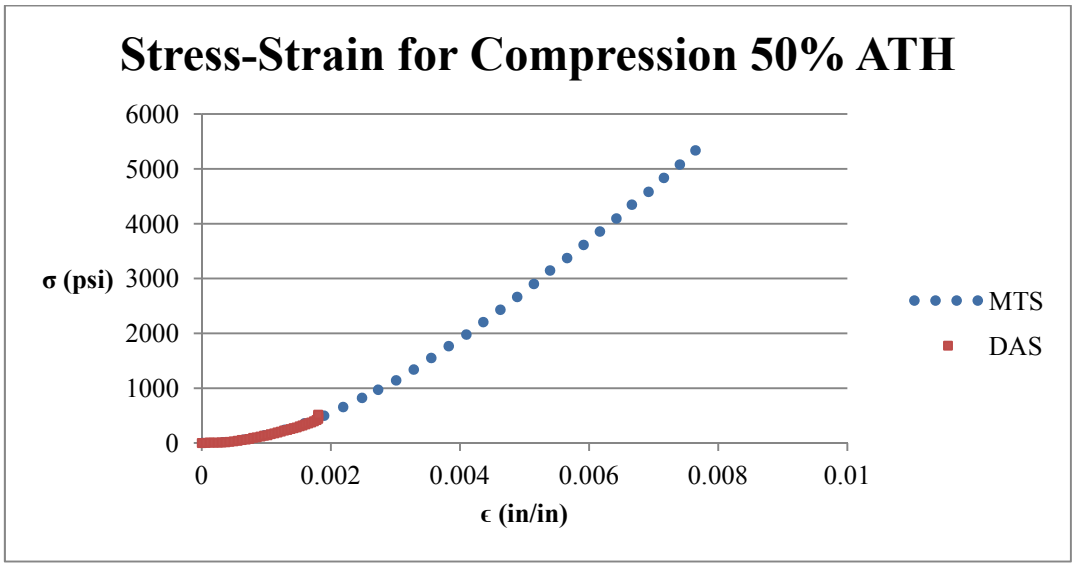

Figure 37: Comparison of Stress-Strain Curves of MTS and DAS for 50% ATH

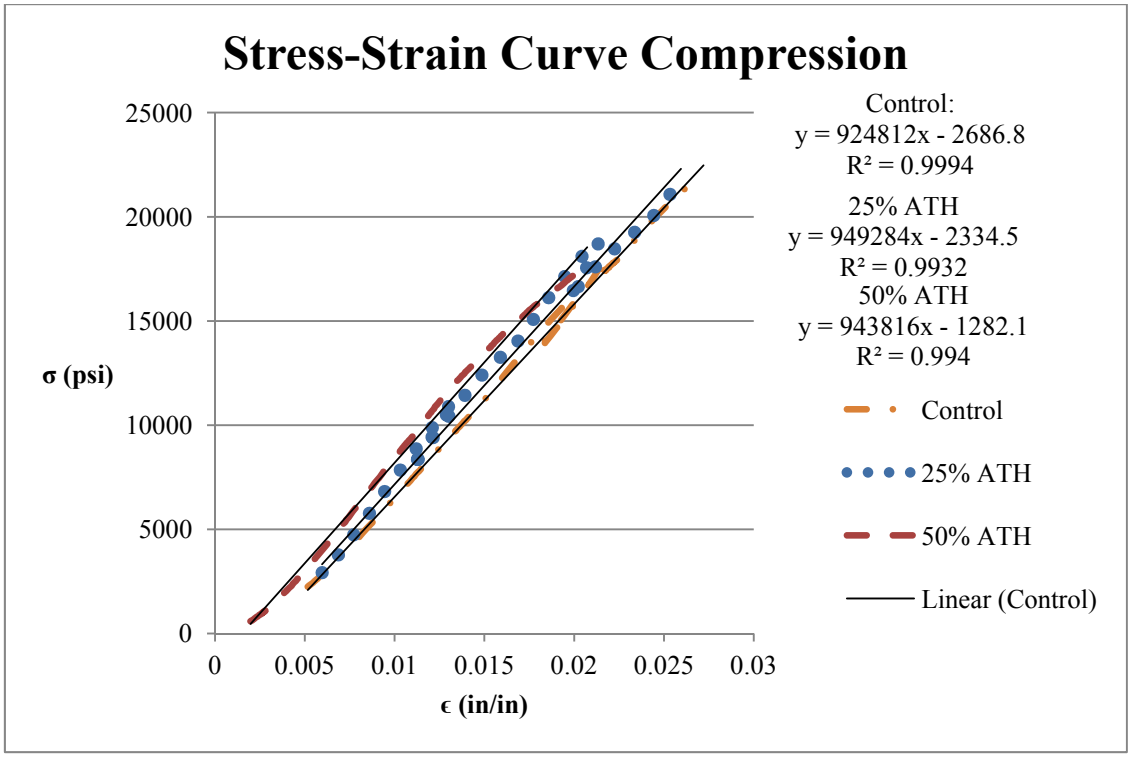

Figure 38: Stress-Strain Curves for Compression

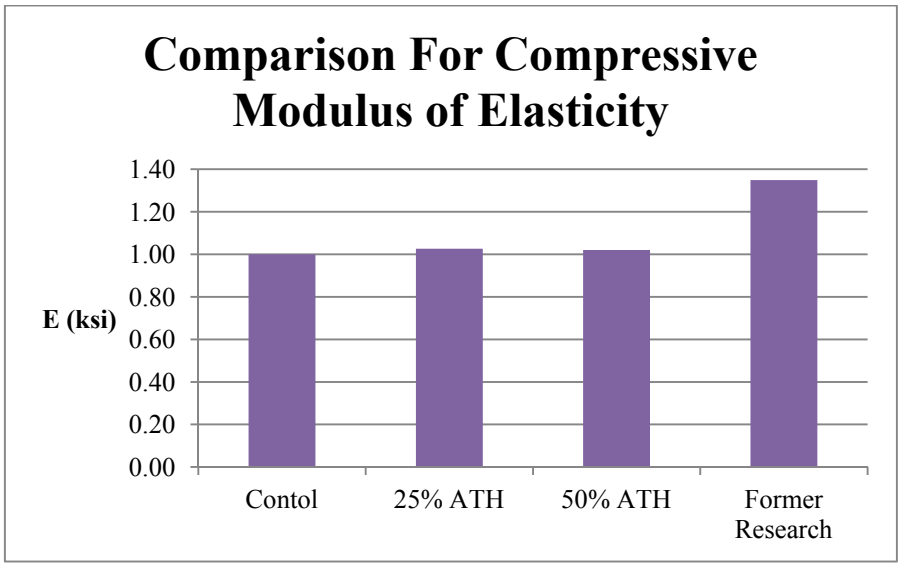

Figure 39: Comparison for Compressive Modulus of Elasticity

Table 25: Maximum Force, Stress and Displacement for Compression

	Control			Previous Research:		
	Average:	STDEV:	COV (%):	Average:	STDEV:	COV (%):
Max Load (lbs):	3684	294	8	---	---	---
Max Stress (psi):	25881	2433	9	21475	580	2.7
Max Δ (in):	0.105	0.011	11	---	---	---
Max ϵ (in/in):	0.031	0.005	16	---	---	---
E (ksi):	924	---	---	1248	---	---
	25% ATH			50% ATH		
	Average:	STDEV:	COV (%):	Average:	STDEV:	COV (%):
Max Load (lbs):	2945	386	13	3772	590	16
Max Stress (psi):	20174	2441	12	19558	3271	17
Max Δ (in):	0.089	0.010	11	0.100	0.024	24
Max ϵ (in/in)	0.028	0.003	11	0.032	0.008	24
E (ksi):	949	---	---	943	---	---

In Table 25 is shown the values for the maximum force, stress, and displacements for all three additive amounts as well as for from the previous research. The maximum stress for this test as well as the maximum strain and displacement is higher than the previous tests, but they are still within the same range. Table 25 is similar to Figure 34 in that the area has not been taken account in the forces, and therefore indicates that 50 ATH has the highest ultimate load, but when adjusted for the differences in areas, as in the stress-strain curve in Figure 38, it can be seen that this is not the case. From this figure, it can be seen that the composite with the highest maximum stress is the control with an ultimate stress of 24.4 ksi. The next strongest is the 25 ATH which has an ultimate stress of 20.2 ksi, followed by the 50 ATH which has an ultimate stress of 19.6 ksi. Therefore, there is a 17%

reduction in ultimate stress from the control to the 25 ATH, and a 19% reduction from the control to the 50 ATH. However, the maximum deflection is reduced from 0.1 in to 0.089 in from the control to 25 ATH, but then the maximum deflection returns to 0.1 in for the 50 ATH. Therefore, while there is a 3% reduction in deflection from the control to the 25% ATH, there is a 0% reduction from the control to 50% ATH. It should also be noted that while the control has the maximum average stress, when reduced by a standard deviation, the control is within the same range as the 25% ATH and the 50% ATH. The difference in strength can be seen in Figure 40, which shows the average ultimate load and the respective standard deviation for each composite.

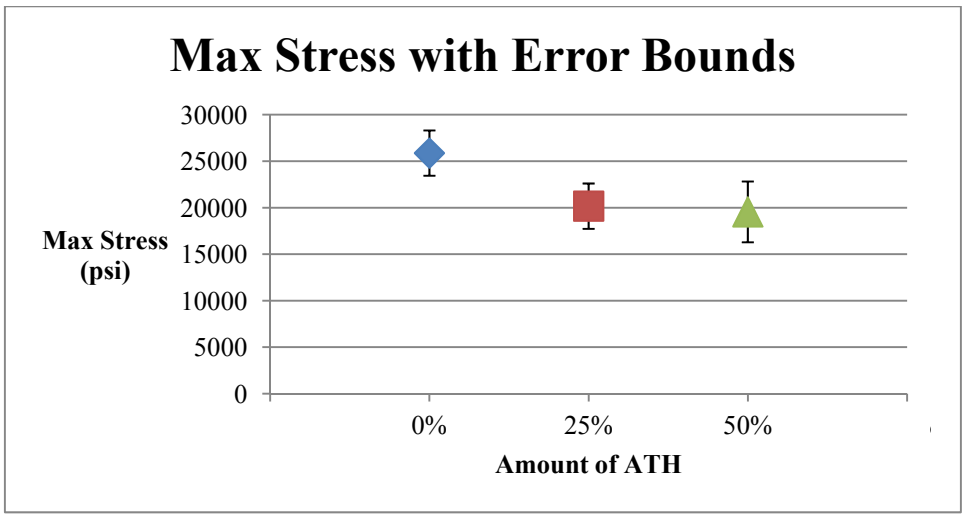

Figure 40: Max Compressive Stress with Error Bounds

5.4.1.2 Failure Mode

There were three crack patterns that occurred in all three ATH amounts. The crack patterns did not seem to have any impact on the maximum strength or maximum displacement of their respective composite groups. The three failure modes can be seen below in Figure 41, in which the cracks have been highlighted with a pink dye for visibility

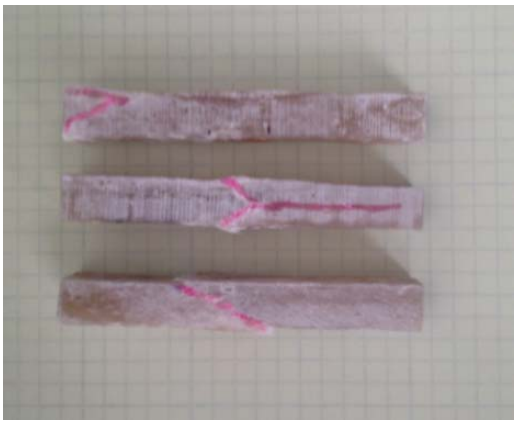

Figure 41: Failure Mode

5.4.2 Flexural (ASTM D 790)

5.4.2.1 Load, Deflection, and Stress

As with the compression tests, a load-displacement curve was developed from the data from the MTS machine, however, due to the nature of the flexural test, stress-strain curves were only created from the data from the DAS combined with the stress data from the MTS, however, no stress-strain curve was developed solely from the MTS data. The stress-strain curves from the DAS can be seen below in Figure 35 and Figure 37, and the force-displacement curve from the MTS can be seen below in Figure 42. Due to problems with the DAS, it only collected one second of data for the 25% ATH and therefore no stress-strain curve was developed from the DAS for the 25% ATH samples. However, stress-strain curves from the DAS were able to be developed for both the control and the 50% ATH samples. Again, like with the compression test, the strain gages stopped working before failure occurred due to debonding. From the linear region in each of the flexural tests, the flexural modulus of elasticity was calculated using Eqs. 5.1-5.2.

$$\Delta = \frac{PL^3}{48EI} \qquad \text{Eq. 5.1}$$

Where Δ is the displacement from the MTS machine (in), P is the force from the MTS machine (lbs), L is the distance between supports on the sample (in), E is the modulus of elasticity (psi), and I is the moment of inertia (in^4) as calculated from Eq. 5.2.

$$I = \frac{bh^3}{12} \qquad \text{Eq. 5.2}$$

From these, the modulus of elasticity was able to be determined from the MTS machine. Then the modulus of elasticity was also determined from the slope of the curves developed from the data from

the DAS. The results from these can be seen below in Table 26, and a percent increase in modulus of elasticity from the control to the other additive amounts may be seen in Figure 45. It should be noted that the modulus of elasticities between the DAS and the MTS are also compared, this is a comparison of increase in modulus of elasticity from the DAS to the respective correlating MTS calculation, therefore, the control is being compared to the control and the 50% ATH is being compared to the 50% ATH. Or in other words, the control DAS is shown as a percent increase from the control MTS. As can be seen, the 50% ATH has the highest modulus, but is very similar to the 25% ATH's. Additionally, the modulus of elasticity for both the control and the 50% ATH calculated from the MTS and has a very good correlation to their modulus of elasticity from the DAS data. Also in Table 26 is summarized the maximum forces, stresses, deflections and the modulus of elasticity from the DAS and the MTS.

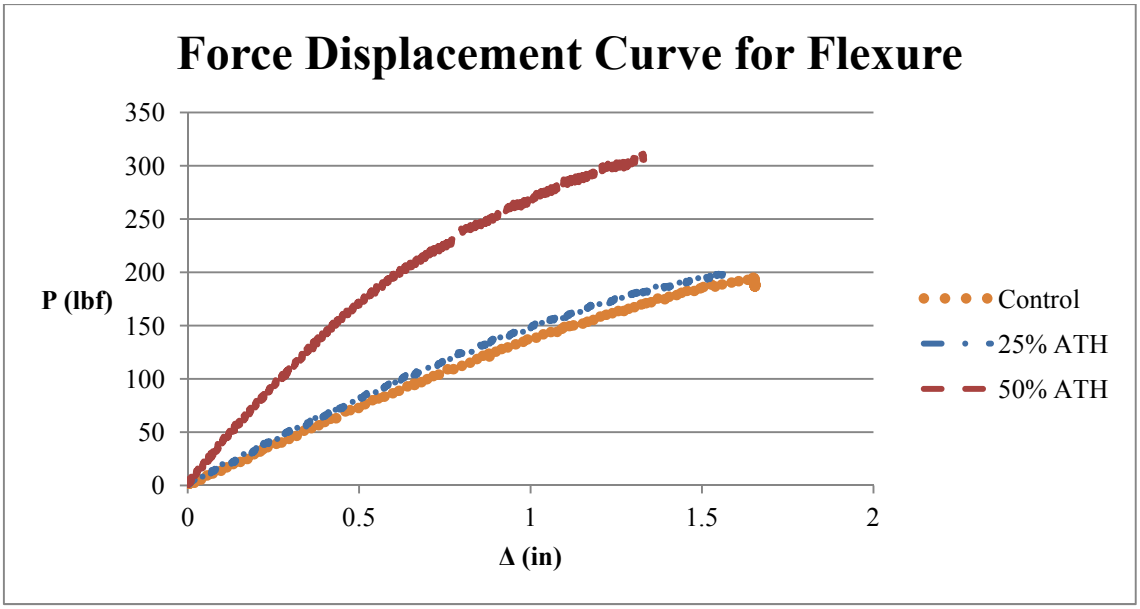

Figure 42: Force-Displacement Curves for Flexure

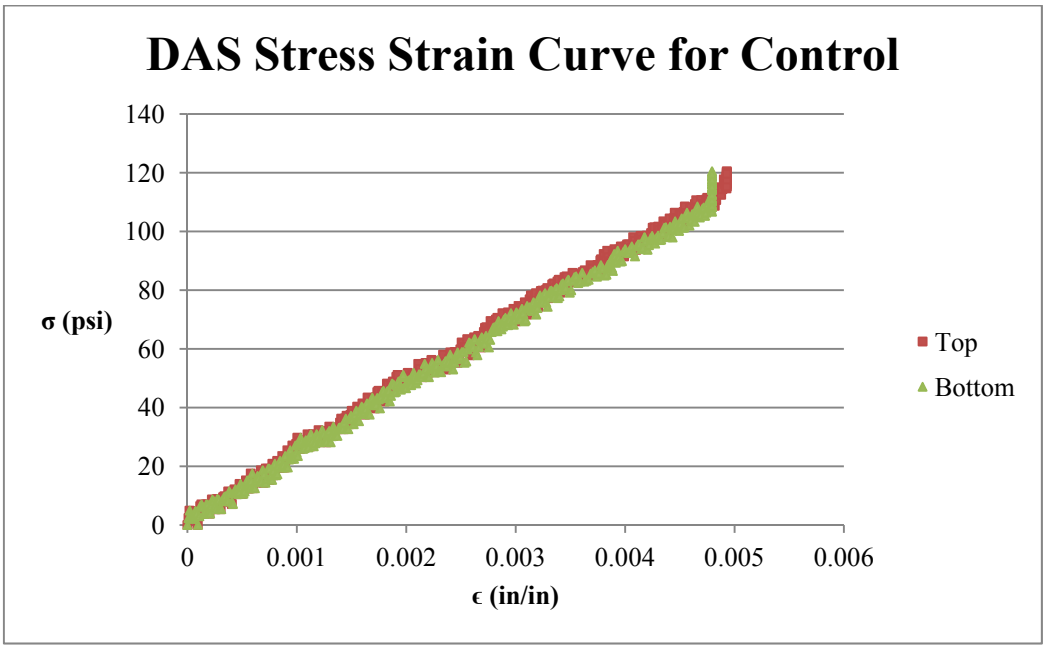

Figure 43: Control Stress-Strain Curve from DAS

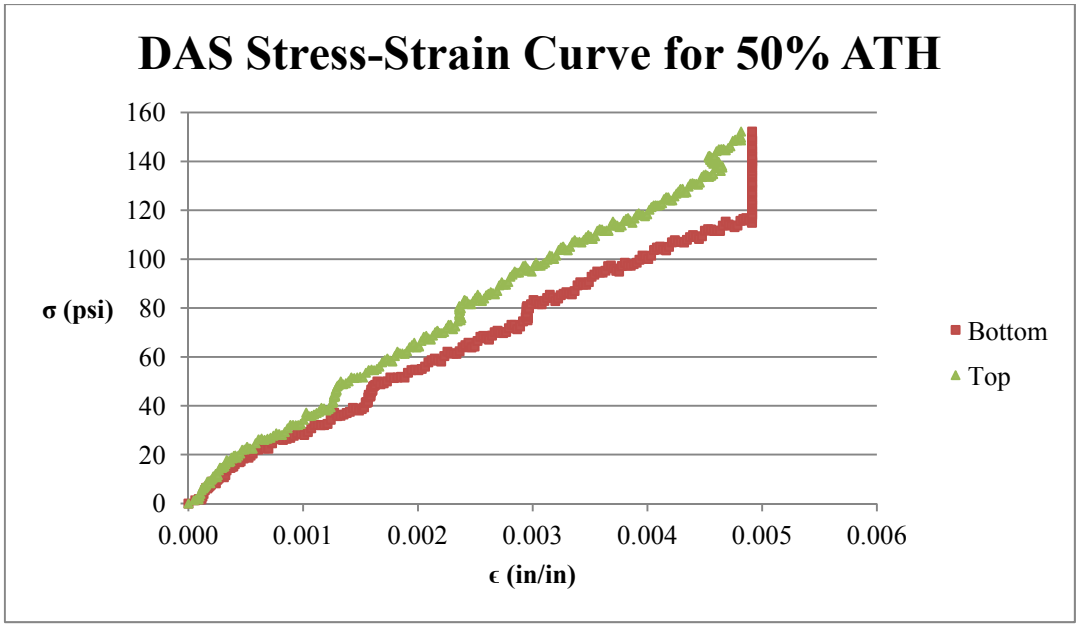

Figure 44: 50% ATH Stress-Strain Curve from DAS

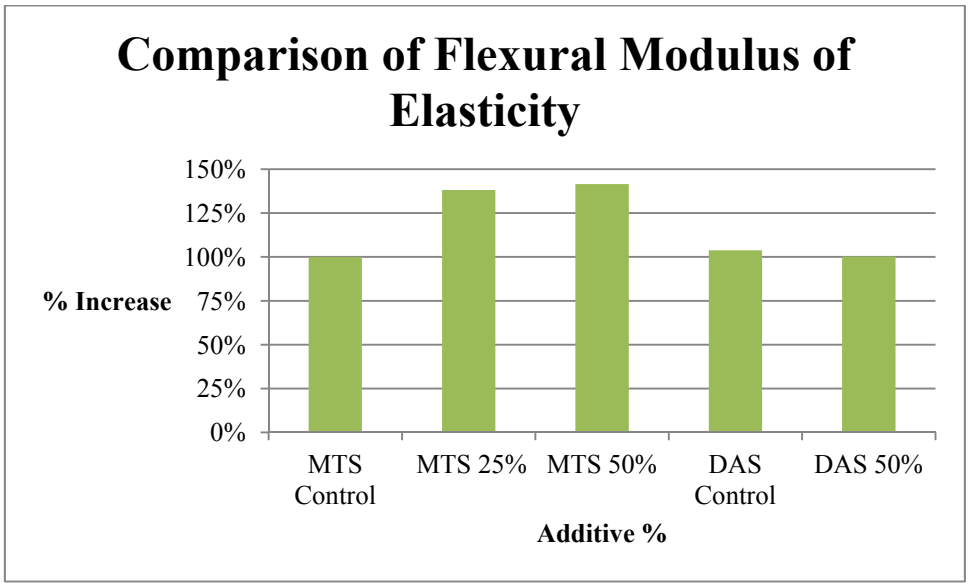

Figure 45: Comparison for Flexural Modulus of Elasticity

Table 26: Average Maximum Force, Stress and Displacement for Flexure

	Control			25% ATH		
	Average:	STDEV:	COV (%):	Average:	STDEV:	COV (%):
Max Load (lbs):	196	1.0	0.5	211	22.3	11
Max Stress (psi):	334	31.2	9	358	14.7	4
Max Δ (in):	1.6	0.1	5	1.64	0.10	6
E MTS (psi):	20466	2504	12	28270	3310.7	11.7
E DAS (psi):	21234	3105	17	--	--	--

	50% ATH		
	Average:	STDEV:	COV (%):
Max Load (lbs):	297	28.5	10
Max Stress (psi):	360	31.7	9
Max Δ (in):	1.3	0.1	9
E MTS (psi):	28976	3216.1	11
E DAS (psi):	29044	2246	8

From Table 26 it can be seen that from the control to 25% ATH, there is an increase of the maximum stress of 7.25% and 0.64% from the 25% ATH to the 50% ATH. When the standard deviations are taken into consideration, all of these regions overlap, but the 50% ATH has the largest possible maximum stress by 19.3 psi. The maximum stresses with their error bounds may be seen below in Figure 46. However, the maximum deflection for the control is 30.26% larger than the 50% ATH, and 0.23% larger than the 25% ATH. For this, the standard deviation for the 25% ATH and the control both overlap, but not for the 50% ATH. The control has the greatest possible deflection, and thus is able to carry the most strain.

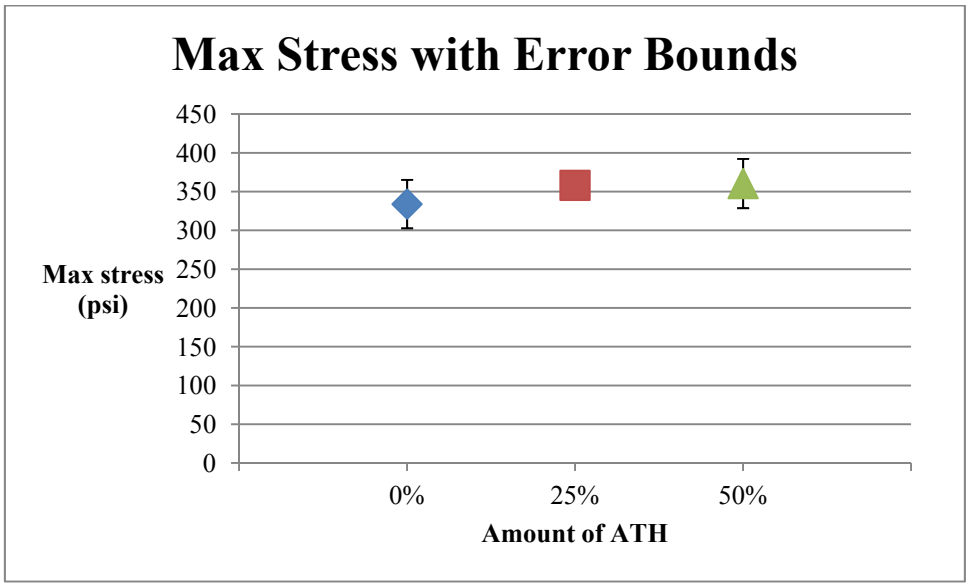

Figure 46: Max Flexural Stress with Error Bounds

5.4.2.2 Failure Modes

The fracture types for all three quantities of ATH were fairly consistent throughout all specimens. The crack first formed at the middle of the 11 inch span, and then propagated both upwards and across the specimen. The result of this may be seen in Figure 47 and Figure 48 where Figure 47 is the bottom of the specimens and Figure 48 is the side of the specimens. The fractures have been dyed pink for better visibility. The failure initiated from the bottom of the specimen and then spread up the sides to the top.

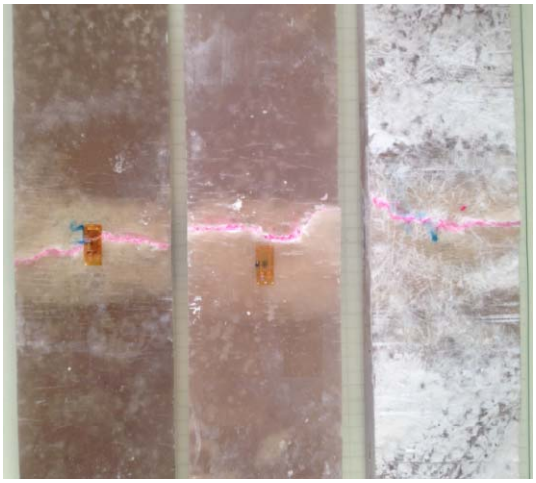

(A) (B) (C)

Figure 47: Failure Mode, Bottom View of (A) Control, (B) 25% ATH, (C) 50% ATH

(A)

(B)

(C)

Figure 48: Failure Mode, Side View of (A) Control, (B) 25% ATH, (C) 50% ATH

5.3.3 Shear (ASTM C 1292)

5.4.3.1 Load, Deflection, and Stress

For the shear tests, six specimen were tested from each type of composite. The force-displacement curve was developed from the data from the MTS machine. The results for each sample were graphed against all the other samples for that additive quantity to ensure that there were no outliers, then tests were repeated as needed to eliminate the outliers. Then the force displacement curves for each different additive amount were graphed together in order to compare the results, this may be seen below in Figure 49. In order to verify the data, the maximum stress was calculated and compared to previous research as can be seen below in Table 27. Due to time constraints, strain gages were unable to be bonded to the shear specimens; therefore no stress-strain curve was developed. In addition, the maximum force, stress and displacement were recorded and are reported below in Table 27, also reported are the standard deviations from the average for each type of resin.

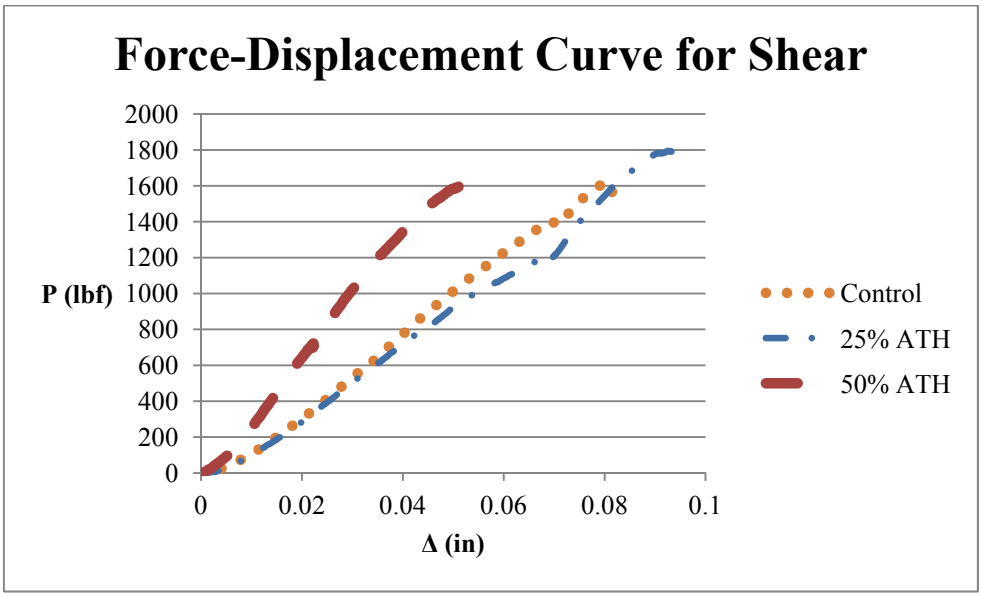

Figure 49: Force-Displacement Curves for Shear

Table 27: Average Maximum Force, Stress and Displacement for Shear

	Control			Previous Research		
	Average:	STDEV:	COV (%):	Average:	STDEV:	COV (%):
Max Load (lbs):	1521	89	6	--	--	--
Max Stress (psi):	11581	675	6	10237	406	4
Max Δ (in):	0.077	0.010	13	--	--	--
	25% ATH			50% ATH		
	Average:	STDEV:	COV (%):	Average:	STDEV:	COV (%):
Max Load (lbs):	1562	213	14	1639	188	11
Max Stress (psi):	11421	1344	12	8470	767	9
Max Δ (in):	0.079	0.011	14	0.061	0.013	21

Below in Figure 50 is shown the difference in maximum stress between each of the different additive amounts. From this as well as from Table 27, the difference in maximum load may be seen. It should be noted that again the 50% ATH samples were thicker, and therefore carry a larger load because of there being no adjustment for area. However, even with that being the case, from the control to the 50% ATH there was a reduction in maximum load of 7.2%. From the control to the 25% ATH there was only a reduction in strength of 2.6%. In addition, the control had the largest deflection with a 6.35% increase from the 25% ATH and a 30.41% increase from the 50% ATH. When the standard deviations are taken into account for stress, the control and the 25% ATH have overlapping bounds, while the 50% ATH and the 25% ATH do not, and therefore neither do the 50% ATH nor the control.

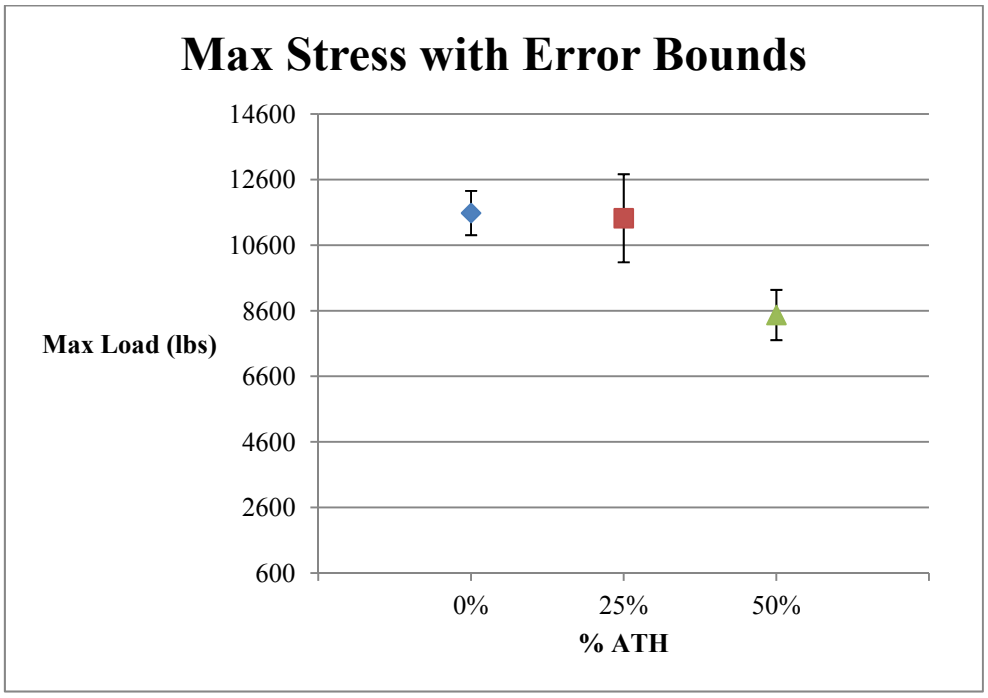

Figure 50: Max Shear Stress with Error Bounds

5.4.3.2 Failure Mode

The three different loading amounts all had slightly different failure types as can be seen in Figure 51. The control failed with no sign of delamination, while both 25% and 50% ATH had shear failures and also slight delamination failures. In addition, the 50% ATH specimen had one sample that had a catastrophic failure. The failure started at the bottom of the specimens at the V-notch, and then propagated up to the top of the specimen.

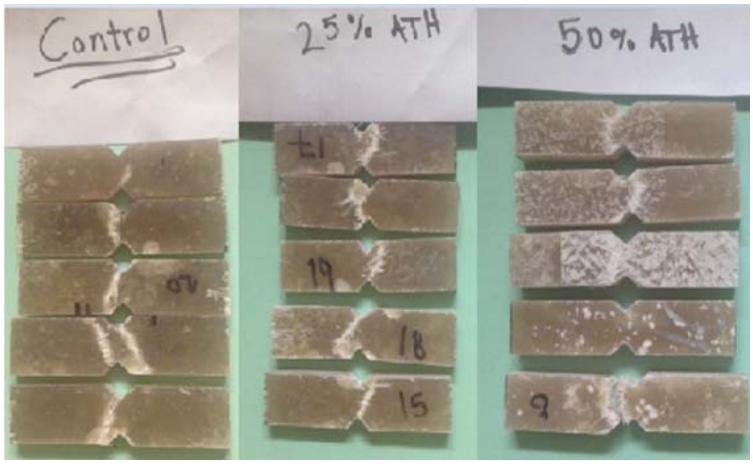

(A) (B) (C)

Figure 51: Failure Mode for (A) Control, (B) 25% ATH, (C) 50% ATH

5.4.4 Tension (ASTM D 638)

5.4.4.1 Load, Deflection, and Stress

Similarly to the compression test, a force-displacement curve was created from the data obtained from the MTS machine, and stress-strain curves were developed from both the data from the MTS machine and the DAS. The curves from the MTS machine and DAS were graphed on the same graph for each specimen to ensure accuracy; this can be seen in Figure 53 for the control, Figure 54 for 25% ATH, and Figure 55 for 50% ATH. Also, in Table 28 is presented the modulus of elasticity from the data from the DAS compared to tensile moduli as calculated by the data from the MTS. Unlike the results for compression and flexure, there was no thickness change between the control, 25% ATH, and 50% ATH since they were all cut to have a constant thickness in order to fit in the tension grips. Therefore, the force-displacement curve, as seen in Figure 52, and the stress strain curve as seen in Figure 56 are very similar, and both correctly represent that the 50% ATH is significantly weaker than the other two composites. Also, from Figure 52 and Figure 56, it can be seen that the control and the 25% ATH act in similar fashions, with similar slopes and maximum deflections, stresses, strains, and loads. In Table 28 the differences in strength between all three laminates can be seen, as well as a comparison to the maximum stress from previous tests. In Figure 57, a comparison may be seen of the modulus of elasticity between each different additive amount. All the MTS are a percent increase from the control sample, and all the DAS are a percent increase from their respective MTS counterparts. Therefore, the control DAS is shown as a percent increase from the control MTS.

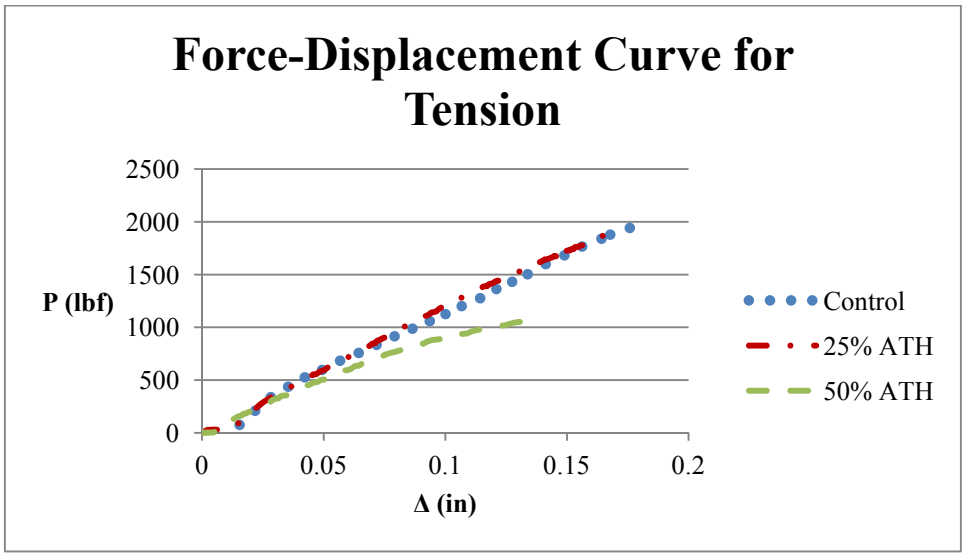

Figure 52: Force-Displacement Curves for Tension

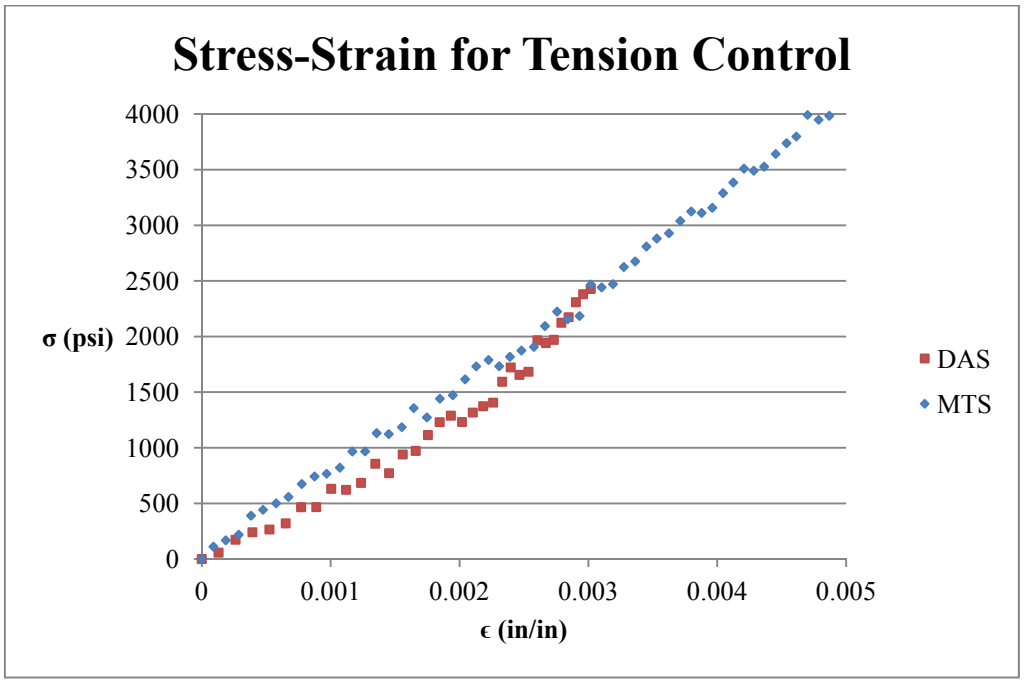

Figure 53: Comparison of Stress-Strain Curves of MTS and DAS for Control ATH

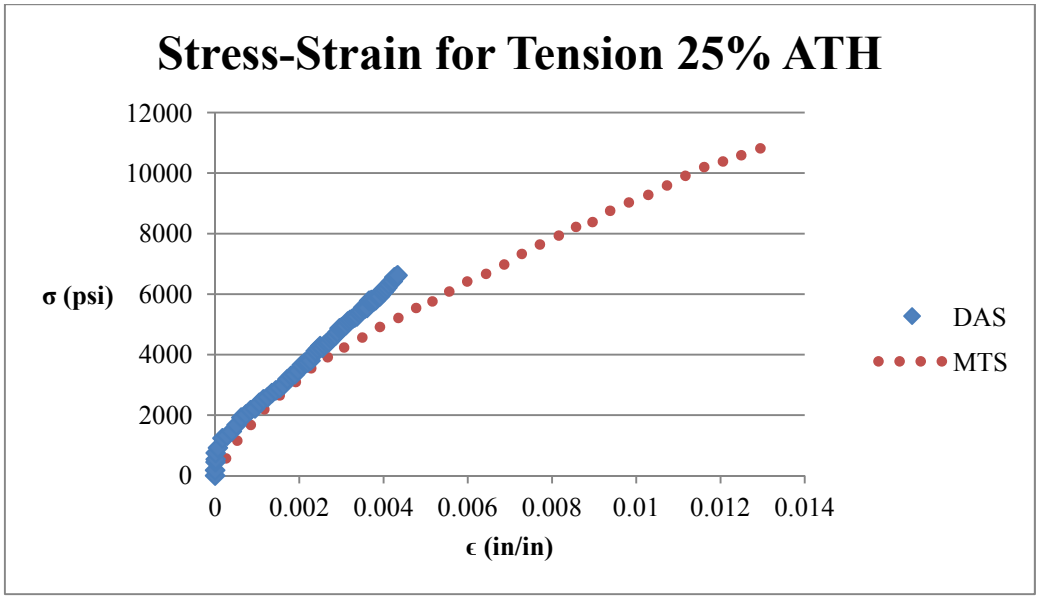

Figure 54: Comparison of Stress-Strain Curves of MTS and DAS for 25% ATH

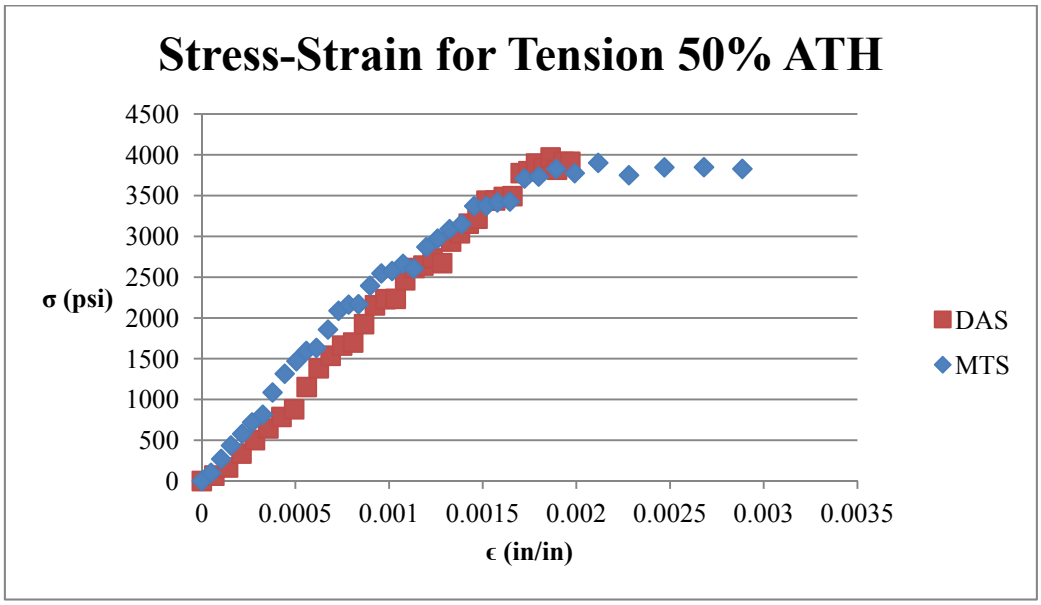

Figure 55: Comparison of Stress-Strain Curves of MTS and DAS for 50% ATH

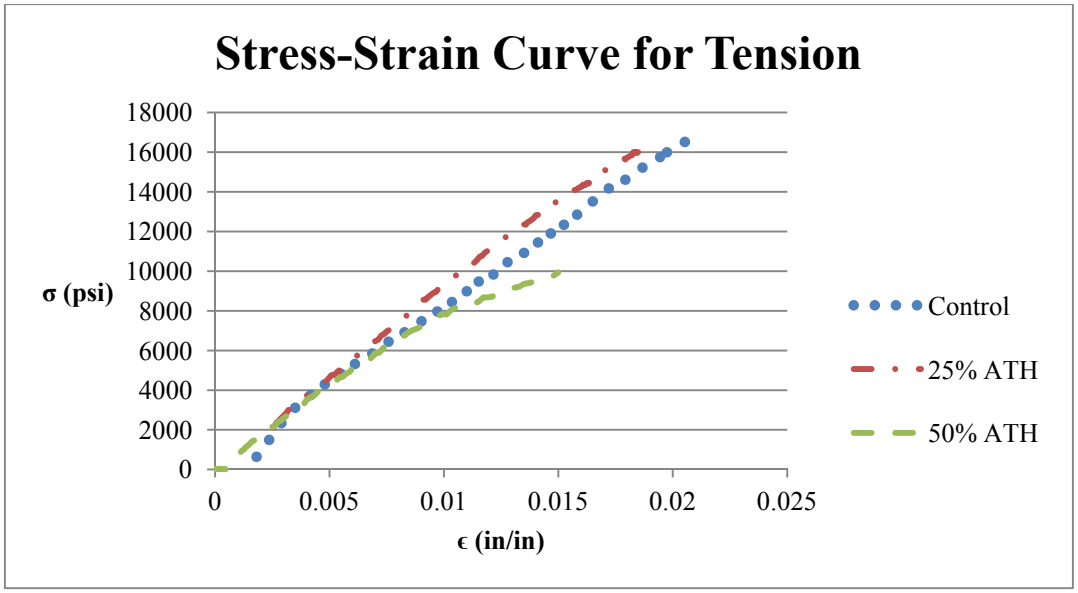

Figure 56: Stress-Strain Curves for Tension

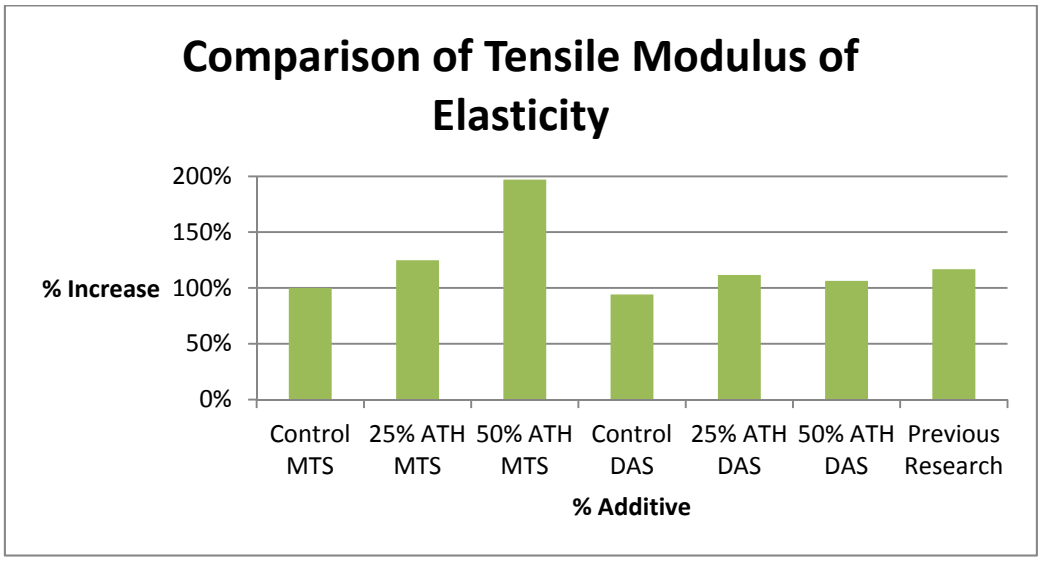

Figure 57: Comparison for Tensile Modulus of Elasticity

Table 28: Average Maximum Force, Stress and Displacement for Tension

	Control			Previous Research		
	Average:	STDEV:	COV (%):	Average:	STDEV:	COV (%):
Max Load (lbs):	1979	82	22	--	--	--
Max Stress (psi):	17308	1154	16	18502	--	--
Max Δ (in):	0.20	0.02	19	--	--	--
Max ϵ (in/in):	0.02	0.002	19	--	--	--
E MTS (ksi):	803	--	--	938	--	--
E DAS (ksi):	757	--	--	--	--	--
	25% ATH			50% ATH		
	Average:	STDEV:	COV (%):	Average:	STDEV:	COV (%):
Max Load (lbs):	1779	236	13	1013	64	6
Max Stress (psi):	16010	708	4	9434	731	8
Max Δ (in):	0.17	0.03	16	0.13	0.01	6
Max ϵ (in/in):	0.02	0.003	16	0.015	0.001	11
E MTS (ksi):	1003	--	--	1583	--	--
E DAS (ksi):	1280	--	--	1685	--	--

From Table 28, it can be seen that the control is able to hold the most load, stress, and has the highest deflection. Its maximum stress is 2% larger than the maximum stress for 25% ATH, and 40% larger than for the 50% ATH. Also, the control's maximum deflection is 6% larger than the 25% ATH, and 23% larger than the 50% ATH. However, with their standard deviations factored in, the 25% ATH falls in the same range as the control for everything, while the 50% ATH does not for maximum load or maximum stress, but does for maximum deflection when compared to both the control and the

25% ATH. Figure 58 presents the difference in maximum stress with error bars for the various additive amount as discussed here.

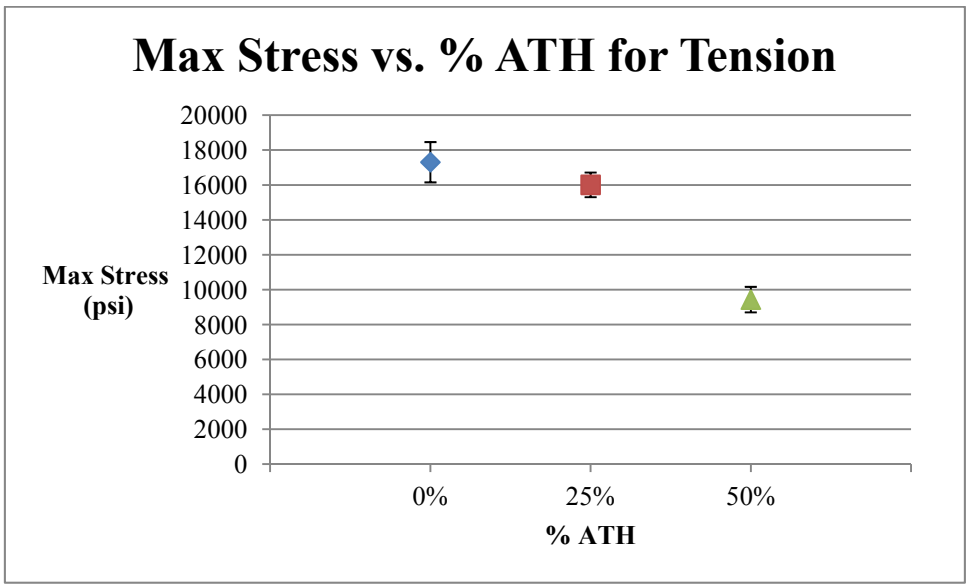

Figure 58: Max Tensile Stress with Error Bounds

5.4.4.2 Failure Mode

For tension, the fracture type was consistent throughout all the resin types. A crack began in the center of the specimen, and then propagated across the 0.5" mid section until pull-apart occurred, as shown in Figure 59.

Figure 59: Failure Mode

5.5 Conclusion

Three layups containing varying amounts of ATH ranging from were tested for their mechanical properties in order to determine the effects ATH had on the mechanical properties of FRP. The tests that were preformed were compression, flexure, shear and tension, and all were preformed according to their respective ASTM standards. From this it was found that for compression, the control is able to hold significantly more stress than the other two laminates. In fact, the control was stronger for all of the tests except for flexure, for which the 50% ATH was the strongest by 0.64% and that the 25%

ATH is 7.25% stronger than the control. However, for shear and tension, the 25% ATH acted very similarly to the control, however, the 50% ATH had a significantly lower maximum stress. Additionally, the modulus of elasticities were compared for all three additive amounts, and it was found that changing the additive amount from the control ratio to 25% ATH had only small changes. Therefore, it may be concluded that using 25% ATH by weight in conjunction with isophthalic resin provides beneficial fire-resistant properties, but also does not have a significant effect of the maximum stress that can be held by the laminate.

Chapter 6 – Conclusions and Recommendations

It was established that there is a need for a polymeric material to be developed which is fire resistant for applications in civil engineering. For the material to be a beneficial building material, the additive which was used to make it fire resistant needed to be both affordable and easy to obtain. Therefore, several additives were tested for time to ignition, time to self extinguish, smoke generation, and smoke color. From the results of these tests it was found that ATH was the optimal additive. ATH was then tested for its effects on flame spread on top of concrete. It was found that ATH in regular isophthalic resin decreased the flame spread compared to isophthalic resin with no ATH added, as well as compared to a fire resistant resin. In order to prevent the FRP was melting in a fire situation, the required thickness of gypsum in order to prevent the FRP from reaching its heat distortion temperature was determined, and it was found that two panels of 5/8" were sufficient from this happening. In order to validate this result, a Comsol model was created, and it was found that the experimental data was accurate. Lastly, the effects on the mechanical properties of the FRP were determined at varying ATH quantities. From these tests, it was determined that when 25% ATH was added to the system, it had little effect on the strength of the composite, however, when 50% ATH was added the maximum stress was significantly reduced.

When 50% ATH was added by weight to the composite, it was not able to sufficiently propagate through the fibers, and therefore the laminate was thicker than the others. However, if the ATH was mixed in at a higher temperature, this would not be a problem as the viscosity of the resin is proportional to temperature. Therefore, additional research is required to determine if this changes the results from the mechanical test, making the 50% ATH the most desirable of the laminates.

Due to time constraints, no strain gage was used for the shear tests. Therefore, in order to compare the shear modulus of elasticity and maximum shear strain, shear tests should be repeated with strain gages.

More tests are also needed to determine the flame spread of the 25% ATH resin on concrete. Flame spread tests were only completed on the 50% ATH resin. Also, thermal tests, such as the cone calorimeter tests, are needed in order to determine how the loading of the resin affects the thermal properties. Lastly, mechanical tests should be performed on the fire-resistant resins to determine how they compare to the regular isophthalic resin.

In all, adding 25% ATH by weight to isophthlalic resin is a cheap and affordable way to provide a fire-resistant system while not drastically changing the mechanical properties of the composite.

Works Cited

Alpolic Materials. (2011). Alpolic/fr Composite Fire Resistive Metal Panels. Mitsubishi Plastics Composites America, Inc.

American Society for Testing and Materials. (2013). Determining Ingnition Temperatures of Plastics. In *ASTM D1929.*

American Society for Testing and Materials. (2013). Determining Water Migration Resistance through Roof Membranes. In *ASTM D 7281.*

American Society for Testing and Materials. (2013). Fire Tests of Building Construction and Materials. In *ASTM E 119.*

American Society for Testing and Materials. (2013). Fire Tests of Roof Coverings. In *ASTM E 108.*

American Society for Testing and Materials. (2013). Stamdard Test Methods for Flexural Properties of Unreinforced and Reinforced Plastics and Electrical Insulating Materials. In *ASTM D 790.*

American Society for Testing and Materials. (2013). Standard Practice for Operating Flourescent Light Apparatus for UV Exposure of Non-Metallic Materials. In *ASTM G 154.*

American Society for Testing and Materials. (2013). Standard Practice for Operating Open Flame Carbon Arc Light Apparatus for Exposure of Non-Metallic Materials. In *ASTM G 152.*

American Society for Testing and Materials. (2013). Standard Practice for Operating Xenon Arc Light Apparatus for UV Exposure of Non-Metallic Materials. In *ASTM G 155.*

American Society for Testing and Materials. (2013). Standard Specifications for Spray Applied Rigid Cellular Polyurethane Insulation. In *ASTM C 1029.*

American Society for Testing and Materials. (2013). Standard Test Method for Compressive Properties of Rigid Plastics. In *ASTM D 695.*

American Society for Testing and Materials. (2013). Standard Test Method for Shear Strength of Continuous Fiber-Reinforced Advanced Ceramics at Ambient Temperatures. In *ASTM C 1292.*

American Society for Testing and Materials. (2013). Standard Test Method for Tensile Properties of Plastics. In *ASTM D 638.*

American Society for Testing and Materials. (2013). Surface Burning Characteristics of Building Materials. In *ASTM E 84.*

American Society for Testing and Materials. (2013). Thermoplastic Fabrics Used in Cold-Applied Roofing and Waterproofing. In *ASTM D 5665.*

American Society for Testing and Materials. (2013). Thermoplastic Fabrics Used in Hot-Applied Roofing and Waterproofing. In *ASTM D 5726.*

Aziz, S. H., Ansell, M. P., Clarke, S. J., & Panteny, S. R. (2005). Modified Polyester Resins for Natural Fibre Composites. *Composites Science and Technology, 65*, 525-535.

Belzer, B. E., Robinson, M. J., & Fick, D. R. (2013). Composite Action of Concrete-Filled Rectangular GFRP Tubes. *Composites for Construction*, 722–731.

Bourbigot, S., Turf, T., Bellayer, S., & Duquesne, S. (2009). Polyhedral Oligomeric Silsesquioxane as Flame Retardant for Thermoplastic Polyurethane. *polymer Degradation and Stability*, 1230-1237.

Chakraverty, A., Mishra, P., & Banerjee, H. (1988). Investigation of combustion of raw and acid-leached rice hush for production of pure amorphous white silica. *Journal of materials Science*, 21-24.

Chand, N., Dan, T., Verma, S., & Rohatgi, P. (1987). Rice husk ash filled-polyester resin composites. *Journal of materials Science Letters*, 733-735.

Chen, A., & Davalos, J. F. (2010). Strength Evaluations of Sinusoidal Core for FRP sandwich Bridge Deck Panels. *Composite Structures*, 1561-1573.

Chowdhury, E. U., Bisby, L. A., Green, M. F., & Kodur, V. K. (2008). Residual Behavior of Fire-Exposed Reinforced Concrete Beams Prestrengthened in Flexure with Fiber-Reinforced Polymer Sheets. *Composites for Construction*, 61-68.

Davalos, J. F., Qiao, P., & Trimble, B. S. (2000). Fiber-Reinforced Composite and Wood Bonded Interfaces: Part1. Durability and Shear Strength. *American Society for Testing and Materials*, 224-231.

Dholakiya, B. Z. (2009). Use of non-traditional fillers to reduce flammability of polyester resin composites. *Kategorizirani Radovi*, 10-17.

Foster, S. K., & Bisby, L. A. (2008). Fire Survivability of Externally Bonded FRP Strengthening Systems. *Composite Construction*, 553-561.

Gibson, R. F. (2007). *Principles of Composite Material Mechanics.* Boca Raton: CRC Press.

Herwig, A., & Motavalli, M. (2012). Axial Behavior of Square Reinforced Concrete Columns Strengthened with Lightweight Concrete Elements and Unbonded GFRP Wrapping. *Composites for Construction*, 747-752.

Kandola, B. K., Horrocks, A. R., Myler, P., & Blair, D. (2002). The Effects of Intumescents on the Burning Behavior of Polyester-Resin-Containing Composites. *Composites: Part A, 33*, 805-817.

Laufer, G., Kirkland, C., Morgan, A. B., & Grunlan, J. C. (2013). Exceptionally flame retardant sulfur-based multilayer nanocoating for polyurethane prepared from aqueous polyelectrolyte solutions. *American Chemical Society Letters*, 361-365.

Manfredi, L. B., Rodriguez, E. S., Wladyka-Przybylak, M., & Vazquez, A. (2006). Thermal degradation and fire resistance of unsaturated polyester, modified acrylic resins and their composites with natural fibres. *Polymer Degradation and Stability*, 255-261.

Materials, A. S. (n.d.). *Standard specifications for spray applied rigid cellular polyurethane insulation.*

Mirmiran, A., Shahawy, M., & Samaan, M. (1999). Strength and Ductility of Hybrid FRP-Concrete Beam-Columns. *Structural Engineering*, 1085-1093.

Mukhopadhyaya, P., Swamy, N., & Lynsdale, C. (1998). Optimizing Structural Response of Beams Strengthened with GFRP Plates. *Composites for Construction*, 87-95.

Nazare, S., Kandola, B., & Horrocks, A. (2006). Flame-retardant unsaturated polyester resin incorporating nanoclays. *Polymers for Advanced Technologies*, 294-303.

Pantelides, C. P., Garfield, T. T., Richins, W. D., Larson, T. K., & Blakeley, J. E. (2012). *Behavior of Concrete Panels Reinforced with Synthetic Fibers, Mild Steel, and GFRP Composites Subjected to Blasts.* Idaho Falls: Idaho National Laboratory.

Reyes, V., Graf, W. P., & Arnold, F. S. (2009). Strengthening of Existing Light-Framed Buildings with Gypsum Shear Walls using a Newly Developed Fiber Reinforced Polymer (FRP)

Assembly. *ATC&SEI Conference on Improving the Seismic Performance of Existing Buildings and Other Structures* (pp. 1204-1212). San Francisco: ASCE.

Thermal Conductivity of some common Materials and Gases. (n.d.). Retrieved from Engineering Toolbox: http://www.engineeringtoolbox.com/thermal-conductivity-d_429.html

Welty, J. R., Wicks, C. E., Wilson, R. E., & Rorrer, G. L. (2008). *Fundamentals of Momentum, Heat, and Mass Transfer.* Hoboken: John Wiley & Sons, Inc.

Wu, L., Hoa, S. V., & Wang, H. (2007). Improvement of Flammability Resistance of Epoxy Adhesives used in Infrastructure Applications. *Canadian Journal of Civil Engineering, 34*, 323-330.

Appendix A – Additional ASTM Standards

In this appendix, the following are the ASTM standards which polymers must adhere to when being used in building applications.

Table 29: Requirements for ASTM C 1029

C 1029							
Material	Compressive Strength (psi)	Thermal Resistance	Water Vapor Permeability (in)	Water Absorption max (%)	Tensile Strength (psi)	Thermal Humid Aging	Closed Cell Content
Type III	40	6.2	3	5	42	6	90
Type IV	60	6.2	3	5	56	5	90

Table 30: Material Requirements

ASTM C 1029							
Material	Compressive Strength (psi)	Thermal Resistance	Water Vapor Permeability (in)	Water Absorption max (%)	Tensile Strength (psi)	Thermal Humid Aging	Closed Cell Content
Type I	15	6.2	3	5	20	12	90
Type II	25	6.2	3	5	32	9	90
Type III	40	6.2	3	5	42	6	90
Type IV	60	6.2	3	5	56	5	90

Table 31: Requirements for ASTM D 1929

Flash Ignition Temperature		Self-Ignition Temperature	
Time	10 mins	Time	10 mins
Temperature (^{o}C)	Increments of 50	Temperature (^{o}C)	Increments of 50

Table 32: Requirements for ASTM D 5665

Types	Unit Mass (g/m^2)	Thickness (mm)	Breaking Load (kN/m)	Elongation (%)	Trapezoid Tearing Strength (N)	Puncture Strength (N)
I: Polyester Spunbonded without resin, unneedled	51	0.21	1.6	32	71	102
II: Polyester spunbonded without resin, needled	119	1.22	4.6	50	142	187
III: Polyester mat plus fiber glass scrim with resin	125	0.41	20.5	3.5	31	53
IV: Polyester core/polyamide sheath bicomponent spunbonded	75	0.56	4.2	24	125	98
V: Polyester mat with polyester sticking	125	0.28	5.6	17	36	329
VI: Polyester amt plus polyester scrim with resin	73	0.12	7	15	44	49
VII: Polyester scrim fabric with resin	58	0.1	6.5	14	76	49

Table 33: Requirements for ASTM D 5726

Types	Unit Mass (g/m^2)	Thickness (mm)	Breaking Load (kN/m)	Elongation (%)	Heat Distortion Stability (%)	Test Temp: 260 °C	Time: Until Specimen is Room Temp
					Trapezoid Tearing Strength (N)	Puncture Strength (N)	
I: Polyester Spunbonded without resin, unneedled	155	0.42	8.8	46		231	2
II: Polyester spunbonded without resin, needled	140	0.51	5.2	25		169	2
III: Polyester mat plus fiber glass scrim with resin	125	0.41	20.5	3.3	31	53	0.2
IV: Polyester core/polyamide sheath bicomponent spunbonded	327	0.92	34	34	256	316	2

Table 34: Requirements for ASTM D 7281

Water Head	Duration of Test	Temperature	Requirement
6 in	7 days	21 ^{o}C	No sign of leakage

Table 35: Requirements for ASTM E 84

Temperature (^{o}F)	Time (mins)
150 ± 5	10

Table 36: Requirements for ASTM E 108

Class	Intermittent Flame Exposure Test				
	Temperature (^{o}F)	Time on (min)	Time off (min)	Cycles	Time after cycles (hr)
A	1400 ± 50	2	2	15	1
B	1400 ± 50	2	2	8	1
C	1300 ± 50	2	2	3	0.5

Spread of Flame Test		Flying Brand Test	
Temperature (^{o}F)	Time (min)	Temperature (^{o}F)	Time (min)
1400 ± 50	10	1400 ± 50	10
1400 ± 50	10	1400 ± 50	10
1300 ± 50	4	1300 ± 50	4

Burning Brand Test	
Temperature of brand(^{o}F)	Time (min)
1630 ± 50	Until brand has been extinguished

Table 37: Requirements for ASTM E 119

Temperature vs Time Data Points		Required Resistance (hr)
Temperature (^{o}F)	Time	1.5
1000	5 min	Maximum Temperature (^{o}F)
1300	10 min	250 above initial temp
1550	30 min	
1700	1 hr	
1850	2 hr	
2000	4 hr	
2300	8 hr	

Table 38: Requirements for ASTM G 152

Spectral Bandpass Wavelength λ in nm	Minimum Percent	Benchmark Solar Radiation - Percent	Maximum Percent
$\lambda < 290$	--	--	4.9
$290 \leq \lambda \leq 320$	2.3	5.8	6.7
$320 < \lambda \leq 360$	16.4	40	24.3
$360 < \lambda \leq 400$	68.1	54.2	80.1

Table 39: Sample of Exposure Cycles for ASTM G 152

Cycle	Filter	Exposure Cycle
1	Daylight	102 min light at 63 ± 3 °C black panel temperature
		18 min light and water spray (air temperature not controlled)
1a	Extended UV	102 min light at 63 ± 3 °C black panel temperature
		18 min light and water spray (air temperature not controlled)
2	Daylight	90 min light, 70 ± 5% RH at 77 ± 3 °C black panel temperature
		30 min light and water spray (air temperature not controlled)
3	Daylight	102 min light at 63 ± 3 °C black panel temperature
		18 min light and water spray (air temperature not controlled)
		Repeat 9 times for a total of 18 h
		Followed by 6 hr dark at 95 ± 4 % RH at 24 ± 2.5 °C
3a	Extended UV	102 min light at 63 ± 3 °C black panel temperature
		18 min light and water spray (air temperature not controlled)
		Repeat 9 times for a total of 18 h
		Followed by 6 hr dark at 95 ± 4 % RH at 24 ± 2.5 °C
4	Daylight	4 hr light at 63 ± 3 °C black panel temperature
		4 hr light and water spray (air temperature not controlled)
5	Daylight	12 hr light at 63 ± 3 °C black panel temperature
		12 hr light and water spray (air temperature not controlled)
6	Window Glass	100% light at 63 ± 3 °C black panel temperature

Table 40: Requirements for ASTM G 154

Spectral Power Distribution of UVA - 340 Fluorescent Lamps			
Spectral Bandpass Wavelength λ in nm	Minimum Percent	Benchmark Solar Radiation - Percent	Maximum Percent
$\lambda < 290$	--	--	0.01
$290 \leq \lambda \leq 320$	5.9	5.8	9.3
$320 < \lambda \leq 360$	60.9	40	65.5
$360 < \lambda \leq 400$	26.5	54.2	32.8
Spectral Power Distribution of UVA - 3351 Lamp for Daylight UV Behind Window Glass			
Spectral Bandpass Wavelength λ in nm	Minimum Percent	Window Glass Filtered Daylight Percent	Maximum Percent
$\lambda < 300$	--	0	0.2
$300 \leq \lambda \leq 320$	1.1	≤ 0.5	3.3
$320 < \lambda \leq 360$	60.5	34.2	66.8
$360 < \lambda \leq 400$	30	65.3	38
Spectral Power Distribution of UVB - 313 Fluorescent Lamps			
Spectral Bandpass Wavelength λ in nm	Minimum Percent	Benchmark Solar Radiation - Percent	Maximum Percent
$\lambda < 290$	1.3	--	5.4
$290 \leq \lambda \leq 320$	47.8	5.8	65.9
$320 < \lambda \leq 360$	26.9	40	43.9
$360 < \lambda \leq 400$	1.7	54.2	7.2

Table 41: Sample of Exposure Cycles for ASTM G 154

Cycle	Lamp	Typical Irradiance	Approximate Wavelength	Exposure Cycle
1	UVA-340	0.89 W/m^2/nm	340 nm	8 hr UV at 60 ± 3 °C black panel temperature
				4 hr condensation at 50 ± 3 °C black panel temperature
2	UVB-313	0.71 W/m^2/nm	310 nm	8 hr UV at 60 ± 3 °C black panel temperature
				4 hr condensation at 50 ± 3 °C black panel temperature
3	UVB-313	0.49 W/m^2/nm	310 nm	8 hr UV at 70 ± 3 °C black panel temperature
				4 hr condensation at 50 ± 3 °C black panel temperature
4	UVA-340	1.55 W/m^2/nm	340 nm	8 hr UV at 70 ± 3 °C black panel temperature
				4 hr condensation at 50 ± 3 °C black panel temperature
5	UVB-313	0.62 W/m^2/nm	310 nm	20 hr UV at 80 ± 3 °C black panel temperature
				4 hr condensation at 50 ± 3 °C black panel temperature
6	UVA-340	1.55 W/m^2/nm	340 nm	8 hr UV at 60 ± 3 °C black panel temperature
				4 hr condensation at 50 ± 3 °C black panel temperature
7	UVA-340	1.55 W/m^2/nm	340 nm	8 hr UV at 60 ± 3 °C black panel temperature
				0.25 hr water spray (no light), temperature not controlled
				3.75 hr condensation at 50 ± 3 °C black panel temperature
8	UVB-313	28 W/m^2/nm	270 to 700 nm	8 hr UV at 70 ± 3 °C black panel temperature
				4 hr condensation at 50 ± 3 °C black panel temperature

Table 42: Requirements for ASTM G 155

Spectral Power Distribution of Xenon Arcs with New or Pre-Aged Filters			
Sprectral Bandpass Wavelength λ in nm	Minimum Percent	Benchmark Solar Radiation - Percent	Maximum Percent
$\lambda < 290$	--	--	0.15
$290 \leq \lambda \leq 320$	2.6	5.8	7.9
$320 < \lambda \leq 360$	28.3	40	40
$360 < \lambda \leq 400$	54.2	54.2	67.5
Spectral Power Distribution of Xenon Arcs with New or Pre-Aged Filters			
Sprectral Bandpass Wavelength λ in nm	Minimum Percent	Window Glass Filtered Daylight Percent	Maximum Percent
$\lambda < 300$	--	0	0.29
$300 \leq \lambda \leq 320$	0.1	≤ 0.5	2.8
$320 < \lambda \leq 360$	23.8	34.2	35.5
$360 < \lambda \leq 400$	62.5	65.3	76.1
Spectral Irradiance for a Xenon Arc with Extended UV Filters			
Sprectral Bandpass Wavelength λ in nm	Minimum Percent	Benchmark Solar Radiation - Percent	Maximum Percent
$250 \leq \lambda \leq 290$	0.1	--	0.7
$290 \leq \lambda \leq 320$	5	5.8	11
$320 < \lambda \leq 360$	32.3	40	37
$360 < \lambda \leq 400$	52	54.2	62

Table 43: Sample of Exposure Cycles for ASTM G 155

Cycle	Filter	Typical Irradiance	Approximate Wavelength	Exposure Cycle
1	Daylight	0.35 W/m^2/nm	340 nm	102 min light at 63 ± 3 °C black panel temperature
				18 min light and water spray (air temperature not controlled)
2	Daylight	0.35 W/m^2/nm	340 nm	102 min light at 63 ± 3 °C black panel temperature
				18 min light and water spray (air temperature not controlled)
				6 hr dark at 95 ± 4 % RH at 24 ± 2.5 °C Unisulated Black
3	Daylight	0.35 W/m^2/nm	340 nm	1.5 hr light, 70 ± 5% RH at 77 ± 3 °C black panel temperature
				0.5 hr light and water spray (air temperature not controlled)
4	Window Glass	0.3 W/m^2/nm	340 nm	100% light at at 63 ± 3 °C black panel temperature
5	Window Glass	1.10 W/m^2/nm	420 nm	102 min light, 35% RH at 63 ± 3 °C black panel temperature
				18 min light and water spray (air temperature not controlled)
6	Window Glass	1.10 W/m^2/nm	420 nm	3.8 hr light, 35% RH at 63 ± 3 °C black panel temperature
				1 hr dark, 90 % RH at 43 °C Black Panel Temperature
7	Extended UV	0.55 W/m^2/nm	340 nm	40 min light, 50 ± 5% RH at 70 ± 2 °C black panel temperature and 47 ± 2 °C Chamber Air Temperature
				20 min light and water spray on specimen face
				60 min light, 50 ± 5% RH at 70 ± 2 °C black panel temperature and 47 ± 2 °C Chamber Air Temperature
				60 min darkand water spray on specimen back 95 ± 5% RH at 38 ± 2 °C black panel temperature and 47 ± 2 °C Chamber Air Temperature

Table 42: Continued

Cycle	Filter	Typical Irradiance	Approximate Wavelength	Exposure Cycle
7A	Daylight	0.55 W/m^2/nm	340 nm	40 min light, 50 ± 5% RH at 70 ± 2 ^{o}C black panel temperature and 47 ± 2 ^{o}C Chamber Air Temperature
				20 min light and water spray on specimen face
				60 min light, 50 ± 5% RH at 70 ± 2 ^{o}C black panel temperature and 47 ± 2 ^{o}C Chamber Air Temperature
				60 min darkand water spray on specimen back 95 ± 5% RH at 38 ± 2 ^{o}C black panel temperature and 47 ± 2 ^{o}C Chamber Air Temperature
8	Extended UV	0.55 W/m^2/nm	340 nm	3.8 hr light, 35% RH at 63 ± 3 ^{o}C black panel temperature 62 ± 2 oC Chamber Air Temperature
				1 hr dark, 95 % RH at 48 ± 3 ^{o}C Black Panel Temperature 38 ± 2 ^{o}C Chamber Air Temperature
9	Daylight	180 W/m^2/nm (at 300 - 400 nm)	300 - 400 nm	102 min light at 63 ± 3 ^{o}C black panel temperature
				18 min light and water spray (air temperature not controlled)
10	Window Glass	162 W/m^2/nm (at 300 - 400 nm)	300 - 400 nm	100% light, 50% R at 89 ^{o}C black panel temperature
11	Window Glass	1.5 W/m^2/nm	420 nm	Continuous light at 63 ^{o}C uninsulated black panel temperature 30% RH
12	Daylight	0.35 W/m^2/nm	340 nm	18 hr consisting of constinuous light at 63 ^{o}C uninsulated panel temperature 30% RH
				6 hr dark at 90 RH at 35 ^{o}C dry bulb temperauture